

This document is confidential and is proprietary to the American Chemical Society and its authors. Do not copy or disclose without written permission. If you have received this item in error, notify the sender and delete all copies.

Experimental and computational studies of the single molecule conductance of Ru(II) and Pt(II) trans-bis(acetylide) complexes

Journal:	<i>Organometallics</i>
Manuscript ID	om-2016-00472k
Manuscript Type:	Article
Date Submitted by the Author:	16-Jun-2016
Complete List of Authors:	Al-Owaedi, Oday; Lancaster University, Physics Costa Milan, David; Liverpool University, Department of Chemistry Oerthel, Marie-Christine; University of Durham, Chemistry Bock, Soren; University of Western Australia, School of Chemistry and Biochemistry Yufit, Dmitry; University of Durham, Chemistry Howard, Judith; University of Durham, Department of Chemistry Higgins, Simon; University of Liverpool, Chemistry Nichols, Richard; Liverpool University, Department of Chemistry Lambert, Colin; Lancaster University, Physics Bryce, Martin; University of Durham, Chemistry Low, Paul; University of Western Australia, School of Chemistry and Biochemistry

SCHOLARONE™
Manuscripts

1
2
3 Experimental and computational studies of the single molecule conductance
4
5
6 of Ru(II) and Pt(II) *trans*-bis(acetylide) complexes
7
8
9

10
11 Oday A. Al-Owaedi,^{a,bθ} David C. Milan,^{cθ} Marie-Christine Oerthel,^{dθ} Sören Bock,^e

12
13 Dmitry S. Yufit,^d Judith A.K. Howard,^d Simon J. Higgins,^c Richard J. Nichols,^{c*} Colin J.

14
15 Lambert,^{a*} Martin R. Bryce,^{d*} Paul J. Low^{e*}
16
17
18
19
20

21 ^a *Department of Physics, University of Lancaster, Lancaster, LA1 4YB, UK*

22
23 ^b *Department of Laser Physics, Women Faculty of Science, Babylon University, Hilla,*
24
25
26 *Iraq.*
27

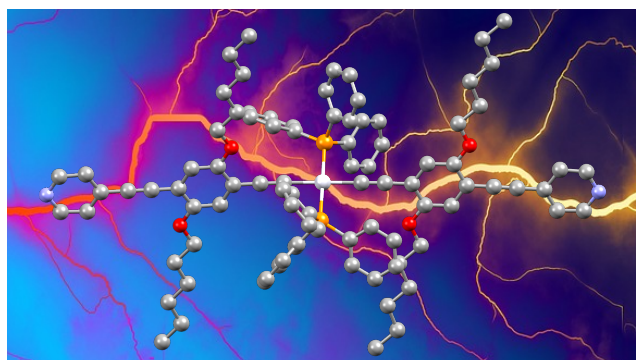
28 ^c *Department of Chemistry, University of Liverpool, Crown St, Liverpool, L69 7ZD, UK*

29
30 ^d *Department of Chemistry, Durham University, South Rd, Durham, DH1 3LE, UK*

31
32
33 ^e *School of Chemistry and Biochemistry, University of Western Australia, 35 Stirling*
34
35 *Highway, Crawley, Perth 6009, Australia*
36
37
38
39

40 *Email: r.j.nichols@liverpool.ac.uk, c.lambert@lancaster.ac.uk,*

41
42 *m.r.bryce@durham.ac.uk, paul.low@uwa.edu.au*
43
44
45
46
47
48
49
50
51
52
53
54
55
56
57
58
59
60



Abstract

The single molecule conductance of metal complexes of general form *trans*-Ru(C≡CArC≡CY)₂(dppe)₂ and *trans*-Pt(C≡CArC≡CY)₂(PPh₃)₂ (Ar = 1,4-C₆H₂-2,5-(OC₆H₁₃)₂; Y = 4-C₅H₄N, 4-C₆H₄SMe) have been determined using the STM *I*(*s*) technique. The complexes display high conductance (Y = 4-C₅H₄N, M = Ru (0.4±0.18 nS), Pt (0.8±0.5 nS); Y = 4-C₆H₅SMe, M = Ru (1.4±0.4 nS), Pt (1.8±0.6 nS)) for molecular structures of ca. 3 nm in length, which has been attributed to transport processes arising from tunneling through the tails of LUMO states.

Introduction

Measurements of the electrical characteristics of a wide variety of saturated, conjugated and redox active organic compounds have served to drive the development of concepts and techniques in molecular electronics.¹⁻³ However, metal complexes offer several potential advantages over organic compounds as components in molecular electronic devices, including redox activity at moderate potentials, ready tuning of frontier molecular orbital energy levels to better match the Fermi levels of metallic electrodes and magnetic properties.^{4,5} Consequently, attention has been turned to the construction and study of metal complexes,⁶⁻¹⁴ clusters,¹⁵⁻¹⁸ extended metal atom chains,¹⁹⁻²¹ and organometallic acetylide species²²⁻³⁴ within molecular junctions.

In the case of purely organic oligo(aryleneethynylene)-based compounds with pyridyl contacting groups, the molecular conductance, as determined by single molecule STM break junction (STM-BJ) experiments, decreases with length, initially in line with the exponential decay expected for a tunneling mechanism before shifting to a shallower length dependence more indicative of an incoherent hopping mechanism of charge transport for compounds of ca. 3 nm in length.³⁵ Conductance values range from $10^{-4.5} G_0$ (2.45 nS) for the 1.6 nm long '3-ring' oligoarylenes $\text{NH}_4\text{C}_5\text{C}\equiv\text{CC}_6\text{H}_2\text{R}_2\text{C}\equiv\text{CC}_5\text{H}_4\text{N}$ (R = OC_6H_{13}) decreasing by approximately three orders of magnitude for the 3.0 nm long '5-ring' system $\text{NH}_4\text{C}_5\text{C}\equiv\text{C}(\text{C}_6\text{H}_2\text{R}_2\text{C}\equiv\text{C})_3\text{C}_5\text{H}_4\text{N}$ ($10^{-6.7} G_0$, 0.015 nS), and thereafter falling only slightly to $10^{-6.9} G_0$ (0.01 nS) in an analogous 5.8 nm long '9-ring' system.

1
2
3 In cases where direct comparison is possible, it has generally been found that the
4
5 incorporation of a ruthenium metal center such as $\text{Ru}(\text{dppm})_2$ ³⁴ or $\text{Ru}(\text{dppe})_2$ ²⁹ within a π -
6
7 conjugated wire-like structure leads to a 2 – 5 fold increase in conductance with the
8
9 conductance value measured likely also being dependent on the nature of the molecule-
10
11 electrode contacting group (e.g. *trans*- $\text{Ru}(\text{C}\equiv\text{CC}_6\text{H}_4\text{SAc})_2(\text{dppm})_2$ STM break junction
12
13 19 ± 7 nS,³⁴ *trans*- $\text{Ru}(\text{C}\equiv\text{CC}_6\text{H}_4\text{C}\equiv\text{CSiMe}_3)_2(\text{dppe})_2$ *I(s)* method $(5.1\pm 0.99) \times 10^{-5}$ G_o /
14
15 3.9 ± 0.8 nS),²⁹ *trans*- $\text{Ru}(\text{C}\equiv\text{C}-4-\text{C}_5\text{H}_4\text{N})_2(\text{dppe})_2$ STM-BJ $(2.5\pm 0.4) \times 10^{-4}$ G_o / 19 ± 3
16
17 nS²⁸).

18
19
20
21
22
23
24
25 In contrast, earlier studies have shown that the Pt(II) complex *trans*-
26
27 $\text{Pt}(\text{C}\equiv\text{CC}_6\text{H}_4\text{SAc})_2(\text{PPh}_3)_2$ behaves rather more as an insulating species when bound
28
29 within a mechanically controlled break junction (MCBJ), with resistances (5 – 50 G Ω ;
30
31 0.2 – 0.02 nS) some three orders of magnitude larger than comparable organic
32
33 compounds $\text{AcSC}_6\text{H}_4\text{C}\equiv\text{CArC}\equiv\text{CC}_6\text{H}_4\text{SAc}$ (Ar = 9,10-C₁₄H₈, 1,4-C₆H₂-2-NH₂-5-NO₂)
34
35 being reported.²² A later study with a range of *trans*- $\text{Pt}(\text{C}\equiv\text{CC}_6\text{H}_4\text{SAc})_2(\text{PR}_3)_2$ complexes
36
37 (R = Cy, Ph, OEt) revealed little effect of the supporting phosphine or phosphite ligand
38
39 on the through-molecule conductance, although curiously the conductance for these Pt
40
41 complexes measured in a cross-wire junction was reported to be some 2 – 3 fold greater
42
43 than that of the simple oligo(phenyleneethynylene) $\text{AcSC}_6\text{H}_4\text{C}\equiv\text{CC}_6\text{H}_4\text{C}\equiv\text{CC}_6\text{H}_4\text{SAc}$.³⁶
44
45
46
47
48
49
50
51

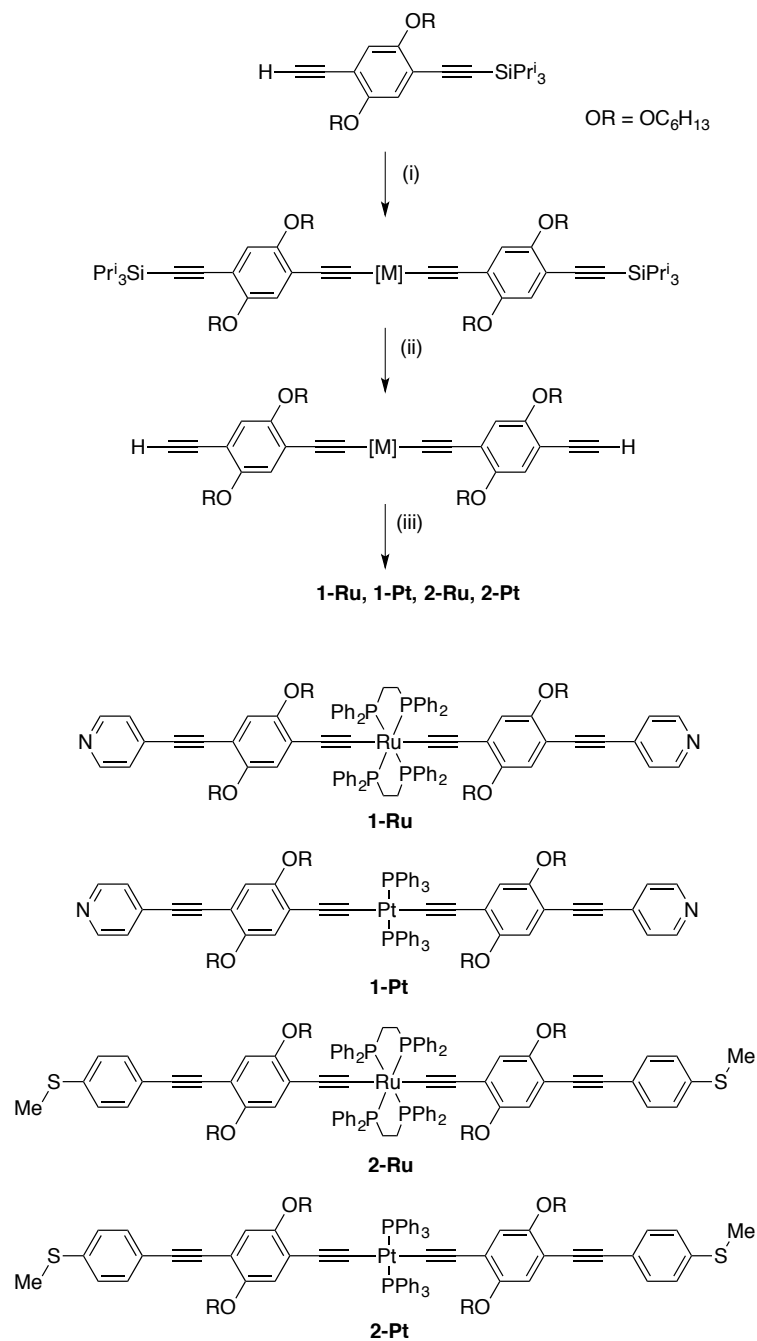
52 Here we turn attention to a family of linearly-conjugated, wire-like organometallic
53
54 complexes featuring *trans*- $\text{Ru}(\text{C}\equiv\text{CR})_2(\text{dppe})_2$ and $\text{Pt}(\text{C}\equiv\text{CR})_2(\text{PPh}_3)_2$ moieties embedded
55
56 within the oligo(aryleneethynylene) backbone of ca. 3 nm molecular length and describe
57
58
59
60

1
2
3 the results of single molecule conductance studies based on the $I(s)$ method. These metal
4
5 complexes are substantially more conductive than their purely organic analogs of
6
7 comparable molecular length, with detailed computational investigation indicating that
8
9 the enhanced conductance arises from conductance through the tails of the LUMO
10
11 resonances. The conductance values obtained from the Pt and Ru systems are remarkably
12
13 similar, suggesting that the readily-synthesized platinum complexes may have an
14
15 important role to play in the further development of metal complexes for applications in
16
17 single molecule electronics.
18
19
20
21
22
23
24
25
26

27 **Results and Discussion**

28
29 Single-molecule measurements using both organic and organometallic compounds have
30
31 clearly shown that the electronic properties of the prototypical metal | molecule | metal
32
33 junctions are strongly influenced by not only the chemical structure of the molecular
34
35 backbone, but are also critically dependent on the combination of the surface and
36
37 contacting groups.³⁷⁻⁴³ The pyridyl-terminated compounds **1-Ru** and **1-Pt** together with
38
39 the analogous methyl thioether-terminated compounds **2-Ru** and **2-Pt** were chosen to
40
41 explore both the relative effects of the Ru(dppe) vs Pt(PPh₃)₂ fragments on molecular
42
43 conductance, and the influence of the electrode-molecule contact in a comparable set of
44
45 compounds. The pyridyl and methyl thioether moieties are already established as surface-
46
47 contacting groups in single-molecule studies of oligoynes and
48
49 oligo(phenyleneethynylenes).^{35, 37, 44-47}
50
51
52
53
54
55
56
57
58
59
60

1
2
3 The complexes **1-Ru**, **1-Pt**, **2-Ru** and **2-Pt** were synthesized in a convergent fashion as
4 indicated in Scheme 1. The precursor terminal alkynyl complexes were assembled from
5 the protected ligand building block 2-triisopropylsilylethynyl-5-ethynyl-1,4-
6 bis(hexyloxy)benzene and [RuCl(dppe)₂]OTf, via a sequence of intermediate vinylidene
7 species which were not isolated but deprotonated in situ, or PtCl₂(PPh₃)₂ through simple
8 CuI-catalysed alkynylation reactions in diethylamine. After removal of the
9 triisopropylsilyl protecting group, the surface binding groups were readily introduced by
10 the ‘on-complex’ cross coupling reactions with 4-iodopyridine or 4-iodothioanisole
11 (Scheme 1).
12
13
14
15
16
17
18
19
20
21
22
23
24
25
26
27
28
29
30
31
32
33
34
35
36
37
38
39
40
41
42
43
44
45
46
47
48
49
50
51
52
53
54
55
56
57
58
59
60



Scheme 1. Synthesis of **1-Ru**, **1-Pt**, **2-Ru** and **2-Pt**. Reagents and conditions: (i) (a) $[\text{RuCl}(\text{dpppe})]\text{OTf}$ / DBU, (b) TlBF_4 (76%) or (a) $\text{cis-PtCl}_2(\text{PPh}_3)_2$ / $\text{CuI}(\text{cat})$ / NHET_2 (81%); (ii) NBu_4F ($[\text{M}] = \text{Ru}(\text{dpppe})_2$ 60%, $\text{Pt}(\text{PPh}_3)_2$ 63%); (iii) 4-iodopyridine /

1
2
3 Pd(PPh₃)₄ /CuI (cat) / NEt₃ (**1-Ru** 64%, **1-Pt** 30%) or 4-iodothioanisole / Pd(PPh₃)₄ /CuI
4
5 (cat) / NEt₃ (**2-Ru** 34%, **2-Pt** 17%)
6
7
8
9

10 The STM *I(s)* technique was used to measure the single-molecule conductance of the
11 series of compounds **1-M** and **2-M** (M = Ru, Pt) in mesitylene solution, with a flame-
12 annealed Au(111) gold-on-glass substrate serving as the bottom electrode and the STM
13 tip creating the top electrode in these elementary metal|molecule|metal junctions. The
14 current is recorded at a fixed bias while the junction is elongated by retraction of the
15 STM tip to generate conductance traces.⁴⁸ From analyses of the conductance traces,
16 break-off distances of 3.1 nm (**1-Ru**) and 3.0 nm (**1-Pt**) can be determined (Table 1). The
17 break-off distance quoted correspond to 95th percentile values from the accumulated *I(s)*
18 scans. These values compare well with the N...N distance obtained from single crystal X-
19 ray diffraction studies of **1-Ru** (Figure 1, 2.86 nm) and **1-Pt** (Figure 2, 2.86 nm), noting
20 that in the solid state these compounds are not perfectly linear, but rather exhibit
21 sigmoidal (**1-Ru**) or gracefully curved (**1-Pt**) structures arising from crystal packing
22 effects. Nevertheless, the good agreement between the break-off distance and the
23 calculated molecular lengths (vide infra) is consistent with the contact of these molecules
24 almost normal to the electrode surface via the pyridine lone pair within these molecular
25 junctions.
26
27
28
29
30
31
32
33
34
35
36
37
38
39
40
41
42
43
44
45
46
47
48
49
50

51 In contrast, shorter break off distances are determined for the methyl thioether complexes
52 **2-Ru** (2.4 nm) and **2-Pt** (2.5 nm, c.f. S...S distance 3.18 nm in the crystallographically-
53 determined molecular structure from a weakly diffracting sample (Figure 3)), which is
54
55
56
57
58
59
60

1
2
3 consistent with a rather more tilted arrangements of the molecule in the junction as might
4
5 be expected from the geometry of the sulfur lone pairs in the thioether,⁴⁹ this
6
7 interpretation has been supported by studies of the DFT-optimized junctions described in
8
9 more detail below.
10
11
12
13
14
15
16
17
18
19
20
21
22
23
24
25
26
27
28
29
30
31
32
33
34
35
36
37
38
39
40
41
42
43
44
45
46
47
48
49
50
51
52
53
54
55
56
57
58
59
60

Table 1. The frontier orbital energies (eV), experimental (Exp. G/G_0) and calculated conductances (Th. G/G_0) at $E_F - E_F^{\text{DFT}} = -0.07$ eV, experimental 95th percentile break-off distance Z^* (nm), molecular length from the DFT-optimized junctions $L = d_{r\dots r}$ (nm), where $r = \text{N}$ or S atoms, bond length between the top gold atoms of gold electrodes and the anchor atoms in the relaxed junctions, X (nm).

Molecule	$E_{\text{HOMO}} /$ eV	$E_{\text{LUMO}} /$ eV	Exp. G/G_0	Th. G/G_0	Z^* (nm)	L (nm)	X (nm)	Contacting Group (Y)
1-Ru	-4.42	-1.46	4.5×10^{-6}	5.4×10^{-6}	3.1	2.9	0.23	4-C ₅ H ₄ N
1-Pt	-4.69	-1.48	9.8×10^{-6}	8.7×10^{-6}	3.0	2.86	0.23	4-C ₅ H ₄ N
2-Ru	-4.18	-1.07	1.8×10^{-5}	1.8×10^{-5}	2.4	2.65	0.245	4-C ₆ H ₄ SMe
2-Pt	-4.40	-1.12	1.8×10^{-5}	1.78×10^{-5}	2.5	2.68	0.245	4-C ₆ H ₄ SMe

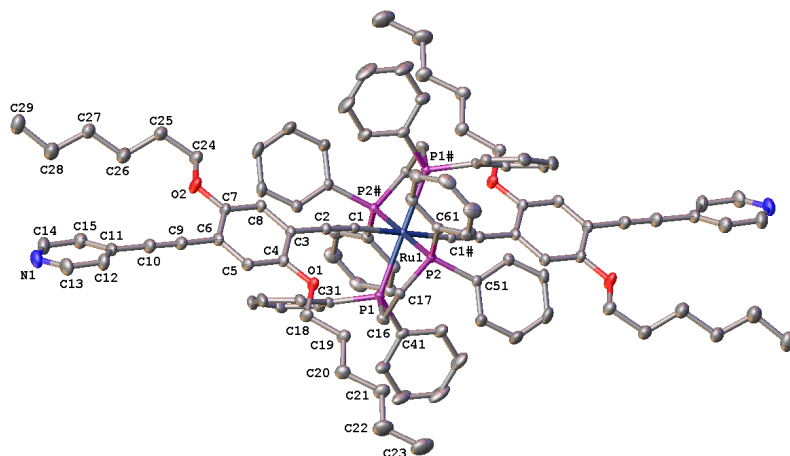


Figure 1. Plot of the molecule **1-Ru** with thermal ellipsoids at 50% probability. Solvent molecules and hydrogen atoms have been omitted for clarity. Torsion angle C(7)-C(6)-C(11)-C(12) : 145.4(2) $^{\circ}$; N(1)-N(1') : 28.624(3) \AA .

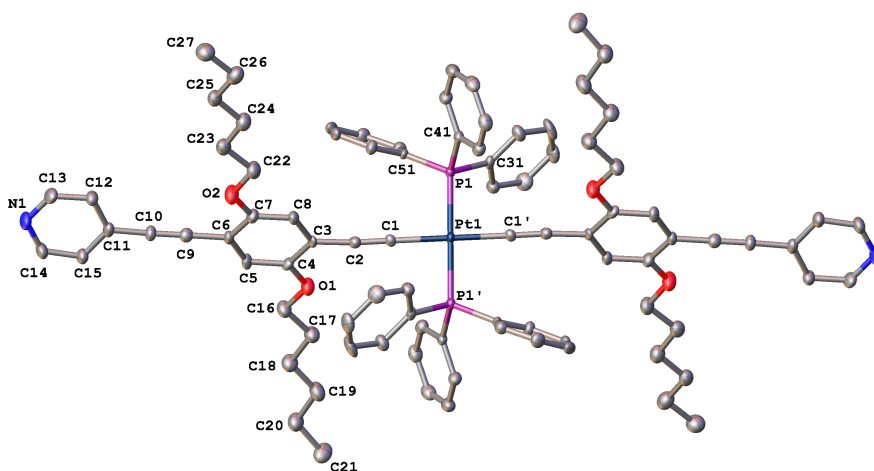


Figure 2. Plot of the molecule **1-Pt** with the thermal ellipsoids at 50% probability. Solvent molecules and hydrogen atoms have been omitted for clarity. Torsion angle C7-C6-C11-C15 164.6(2) $^{\circ}$; N(1)-N(1') : 28.620(7) \AA .

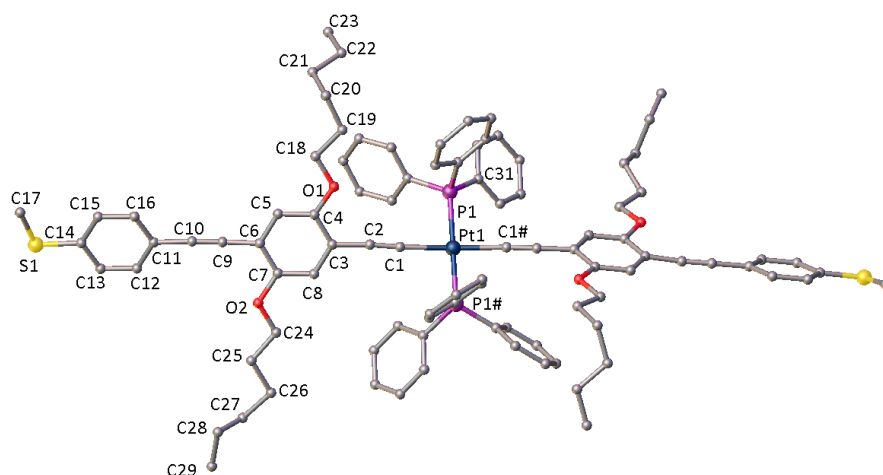
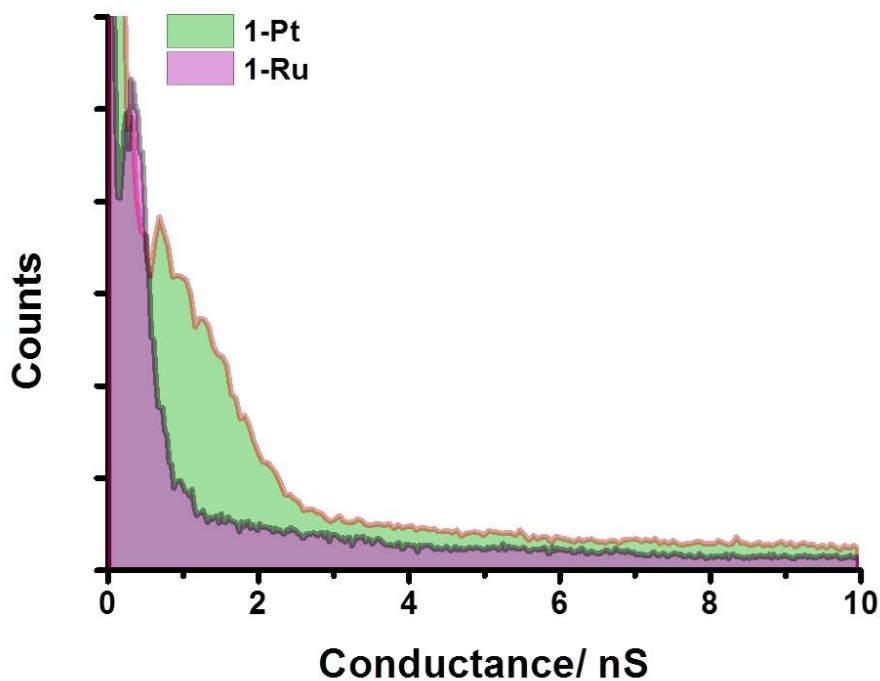


Figure 3. Plot of the molecule **2-Pt**. Solvent molecules and hydrogen atoms have been omitted, and only one component of a disordered hexyloxy side-chain is shown for clarity. Torsion angle C7-C6-C11-C16 165(1)°; S(1)-S(1') : 31.83(2) Å.

The conductance histograms constructed from 500 molecular junction formation traces with characteristic plateaus are shown in Figures 4 and 5. The peak conductance values from these histograms together with key data are summarized in Table 1. These conductance histograms reveal pronounced conductance peaks at 0.4±0.18 nS (**1-Ru**), 0.8±0.5 nS (**1-Pt**), 1.4 ±0.4 nS (**2-Ru**) and 1.8± 0.6 nS (**2-Pt**), and within each pair of compounds featuring the same contacting group these values are indistinguishable. The two- to four-fold increase in conductance values of **2-Ru** and **2-Pt** compared with **1-Ru** and **1-Pt** further indicates the important role of the contacting group in the electrical response of the junction. However, in contrast to the thiolate-contacted molecules derived from *trans*-Ru(C≡CC₆H₄SAc)₂(dppm)₂ (STM-BJ)³⁴ and *trans*-Pt(C≡CC₆H₄SAc)₂(PPh₃)₂ (MCBJ),²² the differences in conductance as a function of the metallic moiety are negligible, and the platinum complexes are as conductive (or resistive) as the ruthenium analogs. The values for **1-Ru** and **1-Pt** whilst low are at least an order of magnitude higher than the ‘five-ring’ organic

1
2
3 compound $\text{NH}_4\text{C}_5\text{C}\equiv\text{C}(\text{C}_6\text{H}_2\text{R}_2\text{C}\equiv\text{C})_3\text{C}_5\text{H}_4\text{N}$ ($\text{R} = \text{OC}_6\text{H}_{13}$; $10^{-6.7} G_0$, 0.015 nS) of
4
5
6 comparable molecular length (3 nm) (MCBJ data).³⁵
7
8
9



33
34 **Figure 4.** $I(s)$ conductance histograms of **1-Ru** and **1-Pt** constructed from 500 traces.
35
36
37

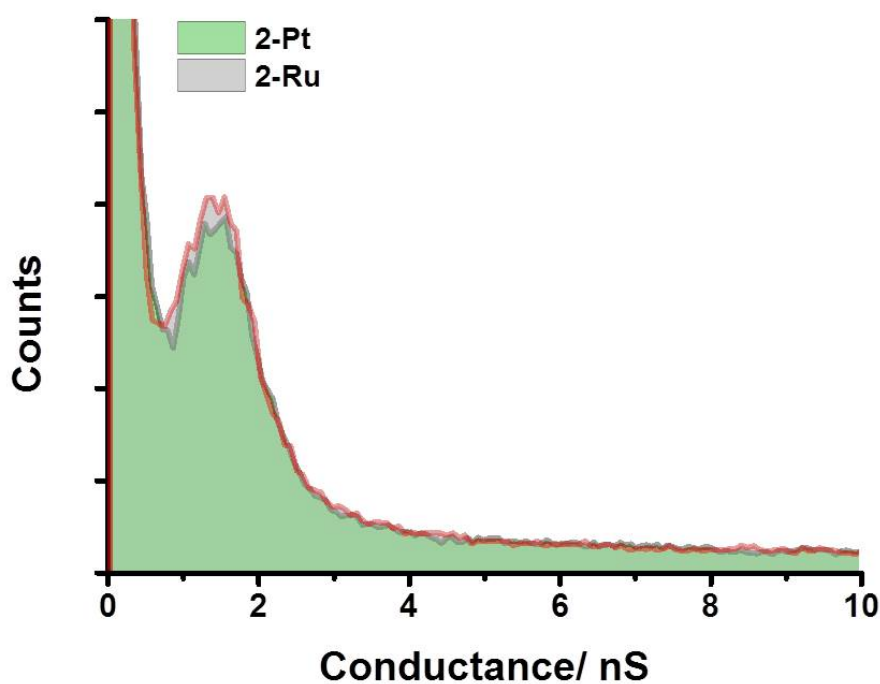


Figure 5. $I(s)$ conductance histograms of **2-Ru** and **2-Pt** constructed from 500 traces.

1
2
3 In seeking to better understand these trends in conductance behavior, the electronic
4 properties of the molecules and the electrical behavior of the junctions have been
5 investigated by using DFT-based methods. Initial studies of the electronic structures
6 of **1-Ru**, **1-Pt**, **2-Ru** and **2-Pt** were carried out at the B3LYP level of theory⁵⁰ with a
7 split LANL2DZ (Ru, Pt) / 6-31G** (all other atoms) basis set.^{51,52} Plots of the highest
8 occupied and lowest unoccupied molecular orbital (HOMO and LUMO, respectively)
9 are given in Figure 6, and analysis of the energy and distribution of the frontier
10 molecular orbitals is summarized in Table 1 and Table 2.
11
12
13
14
15
16
17
18
19
20
21
22
23
24
25
26
27
28
29
30
31
32
33
34
35
36
37
38
39
40
41
42
43
44
45
46
47
48
49
50
51
52
53
54
55
56
57
58
59
60

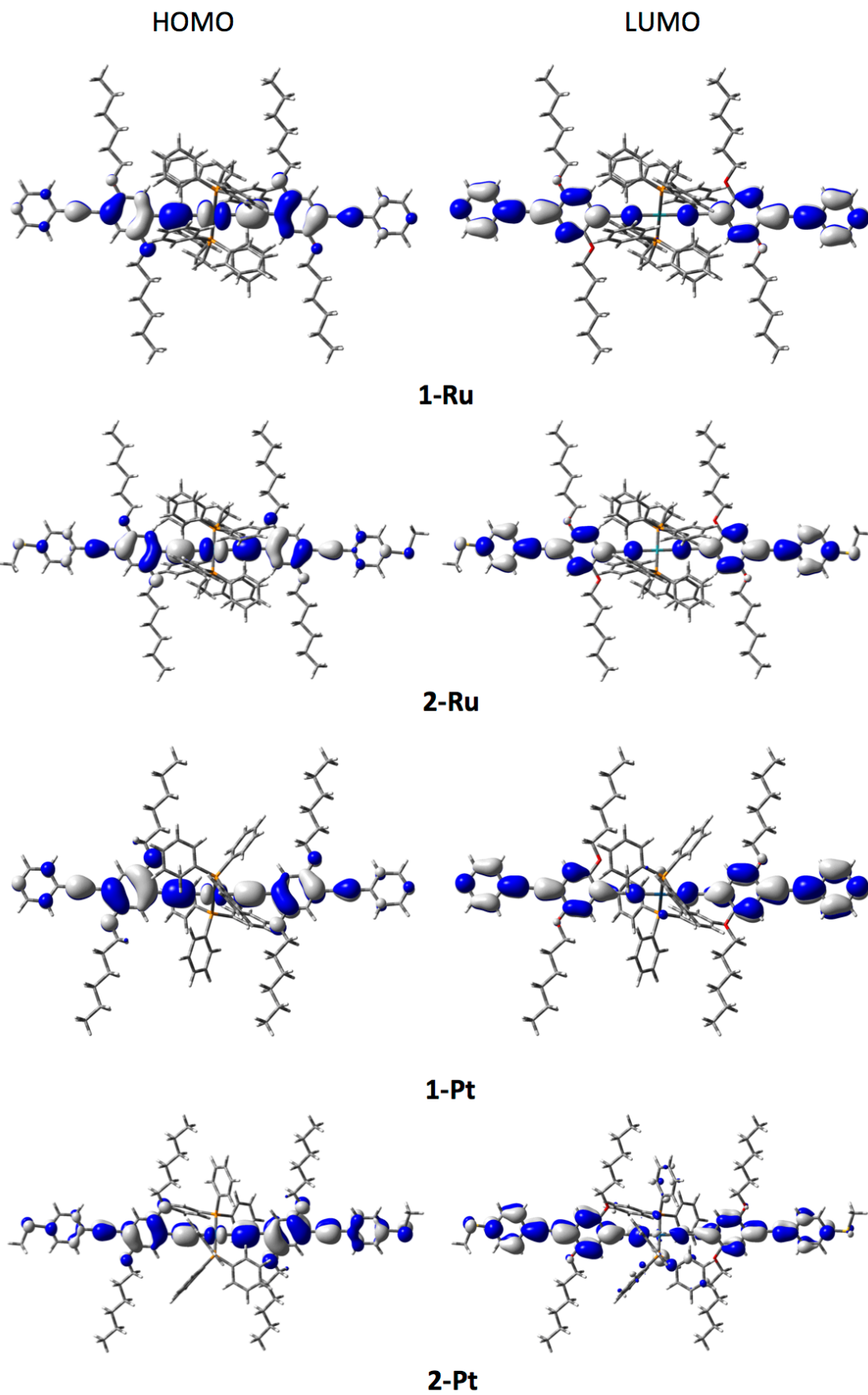


Figure 6. Plots of the HOMO and LUMO of **1-Ru**, **1-Pt**, **2-Ru** and **2-Pt** (isosurfaces ± 0.02 (e/bohr³)^{1/2}).

Table 2 Composition (%) of the HOMO and LUMO of **1-Ru**, **1-Pt**, **2-Ru** and **2-Pt**.

	1-Ru		
	Ru	dppe	C≡CC₆H₄(OC₆H₁₃)₂C≡CC₅H₄N
LUMO	0	2	98
HOMO	25	3	72
	1-Pt		
	Pt	PPh₃	C≡CC₆H₄(OC₆H₁₃)₂C≡CC₅H₄N
LUMO	2	3	95
HOMO	6	2	92
	2-Ru		
	Ru	dppe	C≡CC₆H₄(OC₆H₁₃)₂C≡CC₆H₄SMe
LUMO	0	2	97
HOMO	22	3	76
	2-Pt		
	Pt	PPh₃	C≡CC₆H₄(OC₆H₁₃)₂C≡CC₆H₄SMe
LUMO	4	10	86
HOMO	5	1	94

The HOMOs of the ruthenium complexes display the familiar pattern of $d\pi$ - $p\pi$ interactions along the metal-ethynyl axis,⁵³ and extend along the molecular backbone.

The nodal pattern of the HOMOs in the Pt complexes is similar, with a smaller metal

1
2
3 contribution (Figure 6). The LUMOs are also delocalized over the molecular
4
5 backbones and can largely be described as the π^* system of the diethynylarylene
6
7 ligands with little (Pt) or no (Ru) metal character. These varying metal contributions
8
9 are reflected in the relative orbital energies, with the significant Ru contribution to the
10
11 HOMO in **1-Ru** and **2-Ru** resulting in these orbitals lying some ca. 0.25 eV higher in
12
13 energy than in the Pt analogues **1-Pt** and **2-Pt**. The largely organic π^* based LUMOs
14
15 lead to less significant differences in LUMO energies, which differ by only 0.02 –
16
17
18
19
20
21
22
23
24
25
26
27
28
29
30
31
32
33
34
35
36
37
38
39
40
41
42
43
44
45
46
47
48
49
50
51
52
53
54
55
56
57
58
59
60

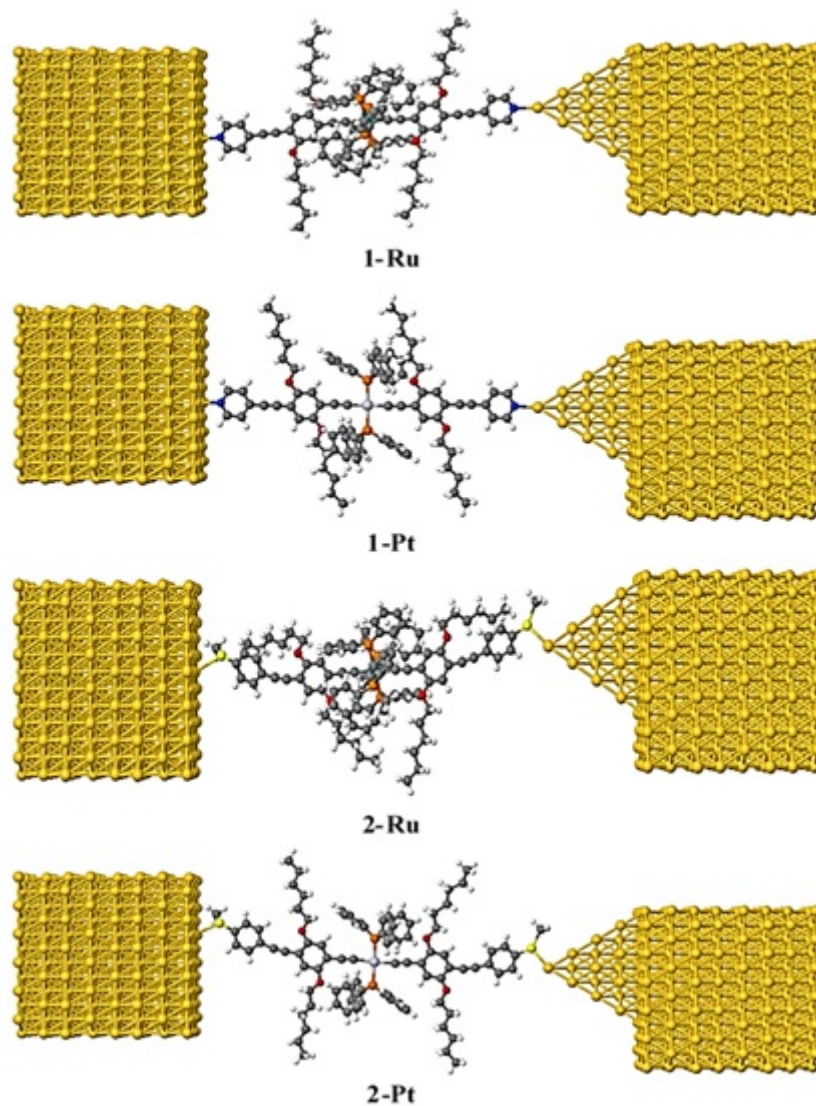
However, these frontier orbital distributions per se do not provide evidence relating to the mechanisms of conductance, which is instead dominated by the alignment of the key molecular orbitals with the Fermi level of the electrodes. As noted by Georgiev and McGrady in computational studies of the conductance properties of extended metal atom chain complexes, the dominant conductance channel need not necessarily be associated with a molecular orbital evenly distributed along the molecular backbone; for example, a dominant conduction channel in $\text{Cr}_3(\text{dpa})_4(\text{NCS})_2$ (dpa = dipyritylamide) is derived from a non-bonding combination of metal d_{z^2} orbitals directed along the Cr-Cr-Cr axis and localized on the terminal chromium atoms.⁵⁴

To provide further insight into the experimentally observed trends obtained using the $I(s)$ technique, and to better evaluate the properties and behavior of these molecular junctions, calculations using a combination of DFT and a non-equilibrium Green's function formalism were also carried out. For the transport calculations, eight layers of (111)-oriented bulk gold with each layer consisting of 6×6 atoms and a layer

1
2
3 spacing of 0.235 nm were used to create the molecular junctions as shown in Figure 7,
4 and described in detail elsewhere.⁵⁵ These layers were then further repeated to yield
5 infinitely-long current-carrying gold electrodes. Each molecule was attached to two
6 (111) directed gold electrodes; one of these electrodes is pyramidal, representing the
7 STM tip, while the other is a planar slab representing the electrode formed by the
8 idealized Au(111) substrate in the $I(s)$ -based molecular junction. The molecules and
9 first layers of gold atoms within each electrode were then allowed to relax again, to
10 yield the optimal junction geometries shown in Figure 7. From these model junctions
11 the transmission coefficient, $T(E)$, was calculated using the GOLLUM code.⁵⁵
12
13
14
15
16
17
18
19
20
21
22
23
24
25
26

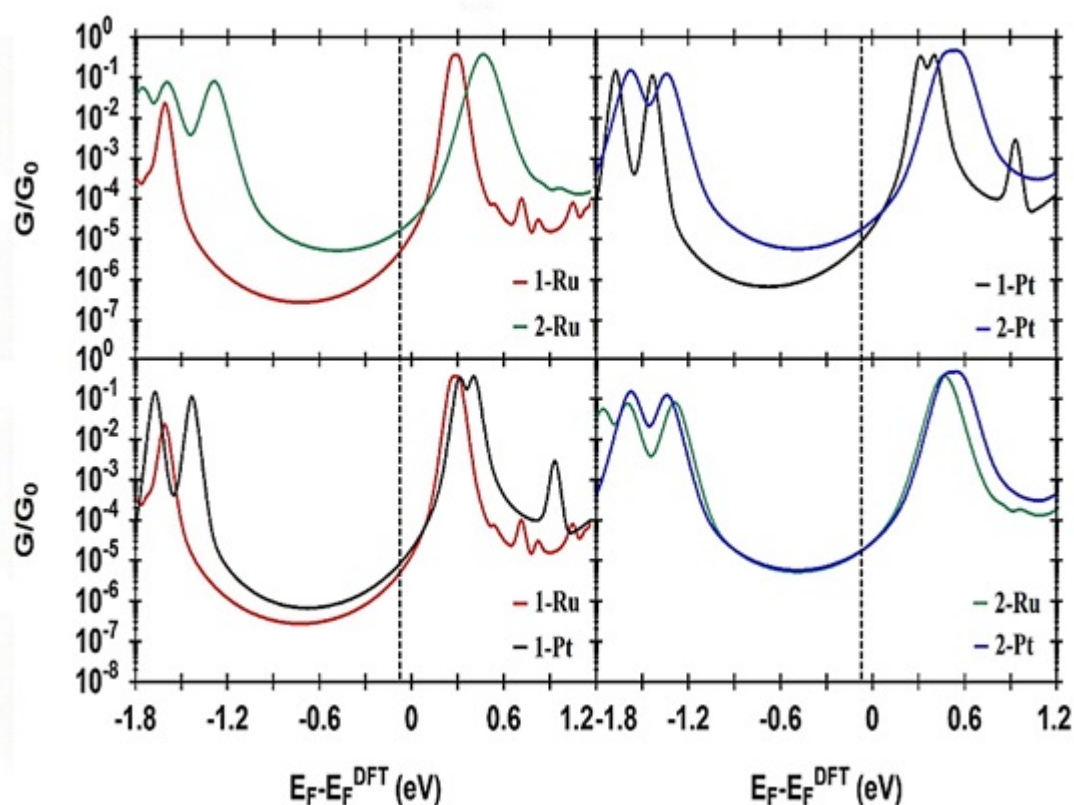
27 It is well-known that the Fermi energy predicted by DFT is often not reliable, and as
28 such the room temperature electrical conductance G was computed for a range of
29 Fermi energies E_F ; the calculated G is plotted as a function of $E_F - E_F^{\text{DFT}}$ in Figure 8.
30 This multi-point fitting of the Fermi energy is a commonly accepted procedure in
31 DFT-based calculations in molecular electronics.⁵⁶ To determine E_F , the predicted
32 conductance values of all molecules were compared with the experimental values and
33 a single common value of E_F was chosen, which gave the closest overall agreement.
34 This yielded a surprisingly small value of $E_F - E_F^{\text{DFT}} = -0.07$ eV, which has been
35 used in all of the theoretical results described below. Thygesen and colleagues have
36 discussed similar situations for C_{60} contacted molecular wires, and shown that critical
37 molecular orbitals can become pinned close to the Fermi level due to partial charge
38 transfer and leading to good quantitative agreement between calculated and
39 experimentally determined conductance.⁵⁷ As shown below, the LUMO states of **1-M**
40 and **2-M** ($M = \text{Ru, Pt}$) tail near the Fermi level in a manner similar to the Thygesen
41
42
43
44
45
46
47
48
49
50
51
52
53
54
55
56
57
58
59
60

1
2
3 system, and partial charge transfer may also be responsible for the good agreement
4
5
6 observed here.
7
8
9
10
11
12
13
14
15
16



58
59
60
Figure 7. The relaxed geometries of molecular junctions of **1-Ru**, **1-Pt**, **2-Ru** and **2-Pt**.

1
2
3
4
5
6 The optimized junction geometries conform well to a description of the pyridine
7
8 contacted compounds **1-Ru** and **1-Pt** forming point contacts between the pyridine
9
10 nitrogen atom and the under-coordinated gold atoms of the gold electrodes. As
11
12 expected, Figure 7 shows that the methyl thioether contacted compounds **2-Ru** and **2-**
13
14 **Pt** are not oriented normal to the idealized, flat electrode surface within the molecular
15
16 junction. Rather, they are tilted within molecular junctions to accommodate the
17
18 directionality of the lone pairs of electrons on the sulfur atoms that bind to the gold
19
20 electrodes.^{49, 58} The calculated molecular lengths and experimental break-off
21
22 distances are consistent with these interpretations (Table 1).
23
24
25
26
27



57 **Figure 8.** Plots showing selected comparisons of calculated conductance as a function
58 of the Fermi energy for molecular junctions **1-Ru**, **1-Pt**, **2-Ru** and **2-Pt**. Black dashed
59 lines show the chosen Fermi energy ($E_F = -0.07$ eV).
60

1
2
3
4
5 The results of the room temperature conductance calculations are summarized in
6
7 Table 1 and comparisons between pairs of molecules according to contacting group
8
9 and metal complex fragment are illustrated in Figure 8. It is immediately apparent that
10
11 the conductance of the methyl thioether-contacted molecules **2-M** is approximately
12
13 three to four times higher than the analogous pyridine contacted species **1-M**, in good
14
15 agreement with the experimental trends (Figure 8, top row, Table 1). The greater
16
17 conductance of the methyl thioether-contacted compounds **2-M** likely arises from the
18
19 greater Au-S bond strength and the broadening of the LUMO resonances arising from
20
21 these interactions versus the pyridine-contacted analogues **1-M**.
22
23
24
25
26
27
28

29 More surprising is the limited influence of the metal-phosphine fragment on the
30
31 molecular conductance (Figure 8, bottom row), which can be explained by the relative
32
33 energy of the Fermi level and the molecular LUMOs together with a conductance
34
35 mechanism based on a tunneling process through the tails of the respective LUMO
36
37 states. Although tunneling through pyridine-terminated compounds is usually
38
39 attributed to LUMO-based transport,^{43, 59, 60} the methyl thioether contact has been
40
41 shown to permit both HOMO- and LUMO-based conductance mechanisms,
42
43 depending on the nature of the molecular backbone.⁶¹ Here it appears that the similar
44
45 conductance values obtained from both series of compounds reflects the similar
46
47 nature, energy and composition of the LUMOs, which provide a conductance channel
48
49 between the electrodes. This contrasts with the recently-reported single-molecule
50
51 conductance studies of *trans*-Ru(C≡CC₃H₄N)(LL)₂ (LL = dppe, dmpe, {P(OMe)₃}₂)
52
53 with the shorter alkynyl pyridine ligands in which the ligand π* levels are likely to be
54
55
56
57
58
59
60

1
2
3 much higher in energy than the extended alkynyl-based ligands in compounds **1-M**
4 and **2-M**, and a HOMO-mediated conductance channel is proposed.²⁸
5
6
7

8
9 In summary, the single molecule conductance of two pairs of *trans*-bis(alkynyl)
10 organometallic complexes based on Ru(dppe)₂ and Pt(PPh₃)₂ fragments and methyl
11 thioether and pyridyl surface contacting groups have been studied in molecular
12 junctions formed by the *I(s)* method. Perhaps surprisingly, the nature of the metal
13 moiety is a less significant point of chemical control over the electrical properties of
14 the junction, with Pt(PPh₃)₂ based complexes being essentially as conductive (or as
15 resistive) as the analogous Ru(dppe)₂ derivatives. The conductance of these
16 compounds is more dependent on the position of the LUMO resonance with respect to
17 the Fermi level of the junction, and largely influenced by the electrode-molecule
18 contact. The energy and distribution of the molecular LUMOs are qualitatively
19 similar in all of the compounds studied here and can be well described as the
20 ethynylarylene ligand π^* orbitals. Given the rather straight-forward synthetic
21 chemistry associated with the preparation of long chain ethynylarylene ligands, this
22 work opens new avenues for the design of metal-complex based molecular wires,
23 including those based on readily-available *trans*-bis(alkynyl) Pt(II) complexes.
24
25
26
27
28
29
30
31
32
33
34
35
36
37
38
39
40
41
42
43
44
45
46
47
48

49 **Acknowledgements** C.J.L. and O.A.A. acknowledge financial support from the
50 Ministry of Higher Education and Scientific Research of Iraq. C.J.L. and M.R.B.
51 acknowledge funding from the EU through the FP7 ITN MOLESCO (project number
52 212942). P.J.L. holds an ARC Future Fellowship (FT120100073) and gratefully
53 acknowledges funding for this work from the ARC (DP140100855). S.B. holds an
54 International Postgraduate Research Scholarship and gratefully acknowledges support
55
56
57
58
59
60

1
2
3 from the University of Western Australia. R.J.N. and S.J.H. thank EPSRC for funding
4 (grant EP/H035184/1 and EP/K007785/1). We thank the Diamond Light Source for
5
6 (grant EP/H035184/1 and EP/K007785/1). We thank the Diamond Light Source for
7
8 an award of instrument time on the Station I19 (MT 6749) and the instrument
9
10 scientists for support.
11

12 13 14 15 EXPERIMENTAL DETAILS

16
17 *General conditions.* All reactions were carried out in oven-dried glassware under
18 oxygen-free argon atmosphere using standard Schlenk techniques. Diisopropylamine
19 and triethylamine were purified by distillation from KOH, other reaction solvents
20 were purified and dried using Innovative Technology SPS-400 and degassed before
21 use. The compounds $[\text{RuCl}(\text{dppe})_2]\text{OTf}$,⁶² *cis*- $\text{PtCl}_2(\text{PPh}_3)_2$ ⁶³ and 1, 4-bis(hexyloxy)-
22 2,5-diiodobenzene⁶⁴ were prepared by literature methods. Other reagents and
23 intermediates were prepared by variations on literature methods as described below,
24 or purchased commercially and used as received.
25
26
27
28
29
30
31
32
33
34
35
36
37
38

39 NMR spectra were recorded in deuterated solvent solutions on Bruker Avance 400
40 MHz and Varian VNMRs 700 MHz spectrometers and referenced against residual
41 protio-solvent resonances (CHCl_3 : ^1H 7.26 ppm, ^{13}C 77.00 ppm and CH_2Cl_2 : ^1H 5.32
42 ppm, ^{13}C 53.84 ppm). In the NMR assignment, the phenyl ring associated with the
43 dppe and PPh_3 are denoted Ph. Ar indicates any arylene group belonging to the
44 alkynyl ligands.
45
46
47
48
49
50
51
52
53
54

55 Matrix-assisted laser desorption ionization (MALDI) mass spectra were recorded an
56 using Autoflex II TOF/TOF mass spectrometer with a 337 nm laser. Infrared spectra
57
58
59
60

1
2
3 were recorded on a Thermo 6700 spectrometer from CH₂Cl₂ solution in a cell fitted
4
5 with CaF₂ windows.
6
7

8
9
10 *2-iodo-5-trimethylsilylethynyl-1,4-bis(hexyloxy)benzene*.⁶⁴ In a 250 mL Schlenk
11 flask, a solution of 1,4-bis(hexyloxy)-2,5-diiodobenzene (6.0 g, 11 mmol),
12 trimethylsilylacetylene (490 mg, 0.7 mL, 5 mmol), PdCl₂(PPh₃)₂ (140 mg, 0.2 mmol),
13 and CuI (38 mg, 0.2 mmol) in degassed dry Et₃N (120 mL) was stirred overnight at
14 room temperature. The solvent was removed and the residue purified on a silica
15 column. Elution with hexane allowed recovery of unreacted 1,4-bis(hexyloxy)-2,5-
16 diiodobenzene, followed by elution with CH₂Cl₂:hexane (1:9), which after
17 evaporation of the solvent produced a yellowish oil of the desired mono-alkyne.
18 Yield: 1.88 g (76 %). ¹H NMR (400 MHz, CDCl₃): δ 7.25 (s, 1H, Ar); 6.83 (s, 1H,
19 Ar); 3.95-3.92 (td, (J = 6.4, 1.4 Hz), 4H, -OCH₂); 1.81 - 1.76 (m, 4H, CH₂); 1.52 -
20 1.48 (m, 4H, CH₂); 1.36 - 1.33 (m, 8H, CH₂); 0.93 - 0.88 (m, 6H, CH₂CH₃); 0.25 (s,
21 9H, SiMe₃) ppm.
22
23
24
25
26
27
28
29
30
31
32
33
34
35
36
37
38
39
40

41 *2-Triisopropylsilylethynyl-5-trimethylsilylethynyl-1,4-bis(hexyloxy)benzene*.²² To a
42 solution of 2-iodo-5-trimethylsilylethynyl-1,4-bis(hexyloxy)benzene (1.88 g, 3.8
43 mmol) in degassed Et₃N (30 mL), triisopropylsilylacetylene (TIPSA) (638 mg, 0.78
44 mL, 3.5 mmol), Pd(PPh₃)₄ (219 mg, 0.19 mmol) and CuI (36 mg, 0.19 mmol) was
45 added. The reaction mixture was stirred overnight at room temperature. The solvent
46 was removed and the residue was purified by passage through a silica pad and elution
47 by ethyl acetate (EtOAc):hexane (1:9) to give a yellow oil, which solidified to give to
48 an off-white colored solid on standing. Yield: 1.30 g (60%). ¹H NMR (400 MHz,
49 CDCl₃): δ 6.88 (s, 1H, Ar); 6.87 (s, 1H, Ar); 3.97 - 3.91 (dt, (J = 12.7, 6.4 Hz), 4H, -
50
51
52
53
54
55
56
57
58
59
60

OCH₂); 1.82-1.72 (m, 4H, CH₂); 1.53 - 1.43 (m, 4H, CH₂); 1.35 - 1.30 (m, 8H, CH₂); 1.13 (s, 21H, SiPr^{*i*}₃); 0.92 - 0.88 (m, 6H, CH₂CH₃); 0.25 (s, 9H, SiMe₃) ppm.

2-Triisopropylsilylethynyl-5-ethynyl-1,4-bis(hexyloxy)benzene (**1**).²² Potassium carbonate (298 mg, 2.16 mmol) was added to a solution of 2-triisopropylsilylethynyl-5-trimethylsilylethynyl-1,4-bis(hexyloxy)benzene (1.20 g, 2.16 mmol) in THF/MeOH (1:1) (160 mL). The solution was stirred for 2 h before CH₂Cl₂ was added. The solution was washed with water, the organic layer was collected and dried over MgSO₄, before the solvent was removed to yield an orange solid, which was used without further purification. Yield: 950 mg (91%). ¹H NMR (700 MHz, CDCl₃): δ 6.91, 6.89 (2 x s, 2 x 1H, Ar), 3.98 (t, (J = 6.5 Hz), 2H, -OCH₂); 3.92 (t, (J = 6.5 Hz), 2H, -OCH₂); 3.31 (s, 1H, C≡C-H); 1.83 - 1.72 (m, 4H, CH₂); 1.49 - 1.44 (m, 4H, CH₂); 1.35 - 1.30 (m, 8H, CH₂); 1.13 (s, 21H, SiPr^{*i*}₃); 0.92 - 0.87 (m, 6H, CH₂CH₃) ppm. ¹³C {¹H} NMR (101 MHz, CDCl₃): δ 154.1 (O-C_{Ar}); 153.9 (O-C_{Ar}); 117.6, 117.2 (HC_{Ar}); 114.6, 112.6 (C_{Ar}); 102.7, 96.6 (C≡); 82.1 (H-C≡); 80.1 (C≡); 69.7, 69.3 (O-CH₂); 31.7, 31.5, 29.4, 29.1, 25.8, 25.6, 22.62, 22.57 (CH₂); 18.7 (H₃C_{SiPr₃}); 14.1, 14.0 (CH₃); 11.4 (HC_{SiPr₃}) ppm.

*Trans-Ru[C≡C{1,4-C₆H₂(OC₆H₁₃)₂}C≡CSiPr^{*i*}₃]₂(dppe)₂* (**2**). The complex salt [RuCl(dppe)₂]OTf (100 mg, 0.09 mmol) was added to a degassed solution of CH₂Cl₂ (4 mL) containing 1,8-diazabicyclo[5.4.0]undec-7-ene (DBU) (4 drops). The solution changed from red to orange with the addition of **1** (96 mg, 0.20 mmol). The reaction mixture was stirred for 1 h at room temperature before TIBF₄ (27 mg, 0.09 mmol) was added. After 20 min, the resulting solution had turned yellow in color and formed a precipitate (TiCl). The precipitate was removed by filtration through a Millex syringe

1
2
3 filter (Millipore) to give an orange solution, which was reduced to the minimum
4
5 volume whereupon methanol (5 mL) was added. A yellow precipitate was obtained
6
7 upon further concentration of the mixture. The product was collected by filtration, and
8
9 dried in air to give **2** as a bright yellow solid. Yield: 131 mg (76%). ^1H NMR (400
10
11 MHz, CDCl_3): δ 7.44 (m, 16H, Ph_o); 7.08 - 7.04 (m, 8H, Ph_p); 6.86 - 6.82 (m, 18H,
12
13 (16H, Ph_m + 2H, Ar); 5.86 (s, 2H, Ar); 3.84 (t, (J = 6.9 Hz), 4H, O- CH_2); 3.64 (t, (J =
14
15 6.4 Hz), 4H, O- CH_2); 2.89 (m, 8H, $\text{PCH}_2\text{CH}_2\text{P}$); 1.73 - 1.61 (m, 8H, CH_2); 1.48 - 1.46
16
17 (m, 4H, CH_2); 1.34 - 1.30 (m, 12H, CH_2); 1.18 (bs, 50H, (42H, SiPr_3^i + 8H, CH_2);
18
19 0.92 (t, (J = 7.0 Hz), 6H, CH_2CH_3); 0.81 (t, (J = 7.0 Hz), 6H, CH_2CH_3) ppm. $^{31}\text{P}\{^1\text{H}\}$
20
21 NMR (162 MHz, CDCl_3): δ 52.07 (s) ppm. $^{13}\text{C}\{^1\text{H}\}$ NMR (101 MHz, CDCl_3): δ
22
23 154.3, 152.6 ($-\text{OC}_{\text{Ar}}$); 137.3 (t, (J = 11.4 Hz), Ph_i); 134.1 (Ph); 128.3 (Ph); 126.8 (Ph);
24
25 121.8 ($\text{C}\equiv$ or C_{Ar}); 117.2, 115.2 (HC_{Ar}); 114.7, 106.5, 104.9, 93.2 ($\text{C}\equiv$ or C_{Ar}); 68.9 (-
26
27 OCH_2); 68.7 ($-\text{OCH}_2$); 31.74 (P- CH_2) overlapping with CH_2 ; 31.69, 29.6, 27.5, 25.9,
28
29 25.8, 22.7, 22.6 (CH_2); 18.8 ($\text{H}_3\text{C}_{\text{SiPr}_3}$); 14.1 (CH_3); 14.0 (CH_3); 11.5 ($\text{HC}_{\text{SiPr}_3}$) ppm.
30
31 IR (CH_2Cl_2): $\nu(\text{C}\equiv\text{CSiPr}_3^i)$ 2138 (m); $\nu(\text{RuC}\equiv\text{C})$ 2050 (s) cm^{-1} . MS^+ (MALDI-TOF;
32
33 m/z): 898.1 $[\text{Ru}(\text{dppe})_2]^+$; 1861.9 $[\text{M}]^+$. HR-ESI $^+$ -MS: m/z calcd for
34
35 $\text{C}_{114}\text{H}_{146}\text{O}_4\text{P}_4^{96}\text{RuSi}_2$ 1856.8895; found 1856.8856.
36
37
38
39
40
41
42
43
44
45

46
47 *Trans-Ru*[$\text{C}\equiv\text{C}-\{1,4-\text{C}_6\text{H}_2(\text{OC}_6\text{H}_{13})_2\}'\text{C}\equiv\text{CH}\}_2(\text{dppe})_2$ (**3**) Tetra-*n*-butylammonium
48
49 fluoride (TBAF) (1.0 M in tetrahydrofuran) (0.24 mL, 0.24 mmol) was added to a
50
51 solution of **2** (180 mg, 0.1 mmol) in THF (15 mL). The solution was stirred overnight
52
53 at room temperature. The resulting mixture was dried and purified on a neutral
54
55 alumina eluted with CH_2Cl_2 :hexane (50:45) with 5% Et_3N to give a yellow solid (100
56
57 mg, 0.06 mmol, 60%). Crystals suitable for X-ray diffraction were grown by slow
58
59 diffusion of MeOH into a CH_2Cl_2 solution of **3** containing 5% Et_3N . ^1H NMR (400
60

1
2
3 MHz, CDCl₃): δ 7.45 - 7.43 (m, 16H, Ph_o) ; 7.09 - 7.05 (m, 8H, Ph_p) ; 6.89 (s, 2H,
4 Ar) ; 6.87 - 6.83 (m, 16H, Ph_m) ; 5.83 (s, 2H, Ar) ; 3.86 (t, (J = 7.0 Hz), 4H, O-CH₂) ;
5
6
7
8 3.67 (t, (J = 7.0 Hz), 4H, O-CH₂) ; 3.31 (s, 2H, C≡C-H) ; 2.93 - 2.89 (m, 8H,
9 PCH₂CH₂P) ; 1.75 - 1.64 (m, 8H, CH₂) ; 1.43 - 1.41 (m, 4H, CH₂) ; 1.36 - 1.30 (m,
10 12H, CH₂) ; 1.23 - 1.20 (m, 8H, CH₂) ; 0.92 (t, (J = 7.0 Hz), 6H, CH₂CH₃) ; 0.82 (t, (J =
11 7.0 Hz), 6H, CH₂CH₃) ppm. ³¹P NMR {¹H} NMR (162 MHz, CDCl₃): δ 51.85 (s)
12 ppm. ¹³C{¹H} NMR (101 MHz, CDCl₃): δ 154.0, 152.6 (-OC_{Ar}) ; 137.2 (t, (J = 15.5
13 Hz), Ph_i) ; 134.1 (Ph) ; 128.4 (Ph) ; 126.9 (Ph) ; 122.3 (C≡ or C_{Ar}) ; 117.7, 115.3
14 (HC_{Ar}) ; 114.5, 104.9 (C≡ or C_{Ar}) ; 81.7 (H-C≡) ; 80.0 (C≡) ; 69.0 (-OCH₂) ; 68.9 (-
15 OCH₂) ; 31.6 (P-CH₂) overlapping with CH₂ ; 31.5, 30.1, 29.5, 29.3, 25.8, 25.6, 22.64,
16 22.58 (CH₂) ; 14.05 (CH₃) ; 14.02 (CH₃) ppm (one quaternary ¹³C≡ was not detected).
17 MS⁺(MALDI-TOF; m/z): 898.0 [Ru(dppe)₂], 1548.4 [M]⁺. IR (CH₂Cl₂):
18 ν(≡CH) 3301 (m); ν(RuC≡C) 2049 (s) cm⁻¹. HR-ESI⁺-MS: m/z calcd for
19 C₉₆H₁₀₆O₄P₄Ru 1548.6113; found 1548.6082.
20
21
22
23
24
25
26
27
28
29

30
31
32
33
34
35
36
37
38
39
40 *Trans*-Ru[C≡C-{1,4-C₆H₂(OC₆H₁₃)₂}C≡CC₅H₄N]₂(dppe)₂ (**1-Ru**). Compound **3** (120
41 mg, 0.077 mmol), 4-iodopyridine (39 mg, 0.192 mmol), Pd(PPh₃)₄ (4.6 mg, 0.004
42 mmol) and CuI (0.8 mg, 0.004 mmol) were added to a degassed solution of NHⁱPr₂
43 (10 mL). The yellow solution was heated at 80 °C for 20 h, during which time the
44 solution turned orange in color with a precipitate developing. The precipitate was
45 removed by filtration and the solid was washed with methanol to remove ammonium
46 salts, to give a yellow powder. Yield: 85 mg (64%). Crystals suitable for X-ray
47 diffraction were grown by slow diffusion of MeOH into a CH₂Cl₂ solution of **1-Ru**
48 containing 5% Et₃N. ¹H NMR (400 MHz, CD₂Cl₂): δ 8.57 (d, (J = 5.2 Hz), 4H,
49 C₆H₄N); 7.52 - 7.40 (m, 16H, Ph_o); 7.37 (d, (J = 5.2 Hz), 4H, C₆H₄N); 7.13 - 7.11 (m,
50
51
52
53
54
55
56
57
58
59
60

1
2
3 8H, Ph_p); 6.95 (s, 2H, Ar); 6.90 - 6.87 (m, 16H, Ph_m); 5.84 (s, 2H, Ar); 3.93 (t, (J =
4 6.5 Hz), 4H, -OCH₂); 3.68 (t, (J = 7.2 Hz), 4H, O-CH₂); 2.96 - 2.93 (m, 8H,
5 PCH₂CH₂P); 1.79 - 1.74 (m, 8H, CH₂); 1.52 - 1.50 (m, 4H, CH₂); 1.38 - 1.36 (m, 12H,
6 CH₂); 1.26 - 1.23 (m, 8H, CH₂); 0.94 - 0.92 (pseudo-t, 6H, CH₂CH₃); 0.84 - 0.82
7 (pseudo-t, 6H, CH₂CH₃) ppm. ³¹P{¹H} NMR (162 MHz, CD₂Cl₂): δ 51.7 (s) ppm.
8
9
10 ¹³C{¹H} NMR (101 MHz, CD₂Cl₂): δ 154.3, 153.3 (-OC_{Ar}); 150.1 (HC_{C₅H₄N}); 137.7
11 (t, (J = 10.9 Hz), Ph_i); 134.5 (Ph); 132.6 (C_{C₅H₄N}); 128.9 (Ph); 127.3 (Ph); 125.4
12 (HC_{C₅H₄N}); 123.3 (C≡ or C_{Ar}); 117.9, 114.9 (HC_{Ar}); 105.3 (C≡ or C_{Ar}); 93.2, 90.7
13 (C≡); 69.4, 69.3 (O-CH₂); 32.1 (P-CH₂); 32.0, 29.5, 29.4, 25.8, 22.7, 22.6 (CH₂); 13.9
14 (CH₃); 13.8 (CH₃) the other quaternary ¹³C≡ were not detected. IR (CH₂Cl₂):
15 ν(C≡CC₅H₄N) 2208 (m); ν(RuC≡C) 2044 (s) cm⁻¹. MS⁺ (MALDI-TOF; m/z): 898.0,
16 [Ru(dppe)₂]⁺; 1702.6, [M]⁺. HR-ESI⁺-MS: m/z calcd for C₁₀₆H₁₁₂N₂O₄P₄⁹⁶Ru
17 1697.6682; found 1697.6688. Anal. Calcd for C₁₀₆H₁₁₂N₂O₄P₄Ru: C, 74.76; H, 6.63;
18 N, 1.64. Found: C, 74.66; H, 6.72; N, 1.70. *Crystal data for 1-Ru*: C₁₀₆H₁₁₂N₂O₄P₄Ru,
19 M = 1524.70, triclinic, space group P-1, a = 12.3676(7), b = 12.9676(7), c =
20 13.9333(8) Å, α = 83.888(2)°, β = 83.489(2)°, γ = 80.585(2)°, U = 2181.4(2) Å³,
21 F(000) = 898.0, Z = 1, D_c = 1.296 mg m⁻³, μ = 0.309 mm⁻¹; 47816 reflections were
22 collected yielding 12134 unique data (R_{int} = 0.0244). Final wR₂(F²) = 0.0952 for all
23 data (531 refined parameters), conventional R₁(F) = 0.0356 for 11015 reflections with
24 I ≥ 2σ, GOF = 1.065.
25
26
27
28
29
30
31
32
33
34
35
36
37
38
39
40
41
42
43
44
45
46
47
48
49
50
51
52
53
54
55

56 *Trans*-Pt[C≡C{1,4-C₆H₂(OC₆H₁₃)₂}C≡CSiPrⁱ₃]₂(PPh₃)₂ (**5**). A mixture of **1** (250 mg,
57 0.52 mmol) and CuI (4 mg) was added to a solution of *cis*-PtCl₂(PPh₃)₂ (200 mg, 0.26
58 mmol) in dry and degassed diethylamine (NHET₂) (20 mL). The orange reaction
59
60

1
2
3 mixture was heated to 100 °C for 2 h. The solvent was removed and the remaining
4
5 residue was purified on a silica column eluted by CH₂Cl₂. The resulting product was
6
7 obtained as an amorphous orange solid. Yield: 320 mg (81%). ¹H NMR (400 MHz,
8
9 CDCl₃) : δ 7.82 - 7.77 (m, 12H, Ph); 7.31 - 7.24 (m, 18H, Ph); 6.63 (s, 2H, Ar); 5.71
10
11 (s, 2H, Ar); 3.60 (t, (J = 6.5 Hz), 4H, O-CH₂); 3.49 (t, (J = 6.8 Hz), 4H, O-CH₂); 1.71
12
13 - 1.63 (m, 4H, CH₂); 1.46 - 1.39 (m, 4H, CH₂); 1.32 - 1.27 (m, 24H, CH₂); 1.10 (s,
14
15 42H, SiPrⁱ₃); 0.91 (t, (J = 7.0 Hz), 6H, CH₂CH₃); 0.86 (t, (J = 7.0 Hz), 6H, CH₂CH₃)
16
17 ppm. ³¹P{¹H} NMR (162 MHz, CDCl₃) : δ 17.43 (s, J_{P-Pt} = 2654.12 Hz) ppm. ¹³C{¹H}
18
19 NMR (101 MHz, CDCl₃): δ 154.1 (-OC_{Ar}); 152.2 (-OC_{Ar}); 135.3 (t, (J = 6.0 Hz), Ph_o);
20
21 131.3 (t, (J = 29.3 Hz), Ph_i); 130.1 (Ph_p); 127.6 (t, (J = 5.4 Hz), Ph_m); 120.9 (C≡ or
22
23 C_{Ar}); 118.9, 116.6 (HC_{Ar}); 109.1, 104.0, 93.8 (C≡ or C_{Ar}); 70.0, 68.9 (O-CH₂); 31.7,
24
25 31.6, 29.5, 29.2, 25.9, 25.5, 22.7, 22.6 (CH₂); 18.7 (H₃C_{SiPr₃}); 14.1 (CH₃) (one
26
27 visible); 11.4 (HC_{SiPr₃}) ppm, the other quaternary ¹³C≡ were not detected. IR
28
29 (CH₂Cl₂): ν(C≡CSiPr₃) 2145 (m); ν(PtC≡C) 2103 (m) cm⁻¹. MS⁺ (MALDI-TOF;
30
31 m/z): 1682.5, [M]⁺. HR-ESI⁺-MS: m/z calcd for C₉₈H₁₂₈O₄P₂¹⁹⁴PtSi₂ 1682.8558;
32
33 found 1682.8484.
34
35
36
37
38
39
40
41
42
43

44 *Trans*-Pt[C≡C{1,4-C₆H₂(OC₆H₁₃)₂}C≡CH]₂(PPh₃)₂ (**6**). A solution of TBAF (1.0 M
45
46 in THF) (0.38 mL, 0.38 mmol) was added to a solution of **5** (150 mg, 0.096 mmol) in
47
48 THF (25 mL). The reaction mixture was stirred for 24 h at room temperature. The
49
50 solvent was removed and the residue re-dissolved in CH₂Cl₂ and washed with water,
51
52 ammonium chloride (NH₄Cl) (aq.) and brine. The organic phase was dried (MgSO₄)
53
54 and the solvent removed to give an amorphous yellow solid. The solid was purified on
55
56 a short silica pad, eluting with 5% NEt₃ in CH₂Cl₂ and compound **6** was obtained by
57
58 precipitation in CH₂Cl₂/MeOH. Yield: 130 mg (63%). ¹H NMR (400 MHz, CDCl₃): δ
59
60

1
2
3 7.83-7.78 (m, 12H, Ph); 7.32-7.25 (m, 18H, Ph); 6.65 (s, 2H, Ar); 5.74 (s, 2H, Ar);
4
5 3.64 (t, (J = 7.0 Hz), 4H, O-CH₂); 3.48 (t, (J = 7.0 Hz), 4H, O-CH₂); 3.19 (s, 2H,
6
7 C≡CH); 1.73-1.66 (m, 4H, CH₂); 1.44-1.40 (m, 4H, CH₂); 1.34-1.13 (m, 24H, CH₂);
8
9 0.91 (t, (J = 6.3 Hz), 6H, CH₂CH₃); 0.86 (t, (J = 6.3 Hz), 6H, CH₂CH₃). ³¹P{¹H}
10
11 NMR (162 MHz, CDCl₃): δ 17.61 (s, J_{P-Pt} = 2648 Hz) ppm. ¹³C{¹H} NMR (101 MHz,
12
13 CDCl₃): δ 153.9, 152.3 (-OC_{Ar}); 135.2 (t, (J = 6.2 Hz), Ph_o); 131.2 (t, (J = 29.3 Hz),
14
15 Ph_i); 130.1 (Ph_p); 127.6 (t, (J = 5.4 Hz), Ph_m); 121.3 (C_{Ar} or C≡); 119.4 (t, (J = 15.1
16
17 Hz), C≡); 118.7, 116.9 (HC_{Ar}); 110.2, 107.6 (C_{Ar} or C≡); 80.9 (H-C≡); 80.4 (C≡);
18
19 69.9, 69.2 (O-CH₂); 31.6, 29.2, 29.1, 25.6, 25.4, 22.61, 22.56 (CH₂); 14.1, 14.0 (CH₃)
20
21 ppm. IR (CH₂Cl₂): ν(C-H) 3300 (w); ν(PtC≡C) 2098 (m) cm⁻¹. MS⁺ (MALDI-TOF;
22
23 m/z): 719.4 [Pt(PPh₃)₂]⁺, 1371.1, [M]⁺. HR-ESI⁺-MS: m/z calcd for C₈₀H₈₈O₄P₂¹⁹⁴Pt
24
25 1369.5863; found 1369.5836.
26
27
28
29
30
31
32
33

34
35 *Trans*-Pt[C≡C{1,4-C₆H₂(OC₆H₁₃)₂}C≡CC₅H₄N]₂(PPh₃)₂ (**1-Pt**). Compound **6** (90 mg,
36
37 0.064 mmol), 4-iodopyridine (30 mg, 0.15 mmol), Pd(PPh₃)₄ (4 mg, 0.003 mmol) and
38
39 CuI (0.8 mg, 0.004 mmol) were added to a Schlenk flask charged with degassed Et₃N
40
41 (10 mL), and the reaction mixture was heated for 2 h at 100 °C. The solvent was
42
43 removed from the yellow solution and the residue purified by column
44
45 chromatography on silica eluting with CH₂Cl₂:hexane:Et₃N (8.5:1.5:0.5) to give a
46
47 yellow solid. The solid was dissolved in the minimum amount of CH₂Cl₂ and MeOH
48
49 (5 mL) was added. Concentration of the solution caused the desired **1-Pt** to
50
51 precipitate. Yield : 30 mg (30%). Crystals suitable for X-ray diffraction were grown
52
53 by slow diffusion of MeOH into a CH₂Cl₂ solution of **1-Pt** containing 5% NEt₃. ¹H
54
55 NMR (400 MHz, CDCl₃): δ 8.54 (pseudo-d, 4H, C₅H₄N), 7.83-7.81 (m, 12H, Ph),
56
57 7.33-7.26 (m, 22H, (18H, Ph + 4H, C₅H₄N), 6.69 (s, 2H, Ar), 5.78 (s, 2H, Ar), 3.68
58
59
60

(pseudo-t, 4H, O-CH₂), 3.53 (pseudo-t, 4H, O-CH₂), 1.76 - 1.72 (m, 4H, CH₂), 1.50 - 1.47 (m, 4H, CH₂), 1.38 - 1.16 (m, 24H, CH₂), 0.92 - 0.85 (m, 12H, CH₂CH₃) ppm. ³¹P{¹H} NMR (162 MHz, CDCl₃): δ 17.67 (s, J_{P-Pt} = 2643.5 Hz) ppm. ¹³C{¹H} NMR (101 MHz, CDCl₃): δ 153.8, 152.5 (-OC_{Ar}), 149.5 (HC_{C₅H₄N}), 135.2 (t, (J = 6.2 Hz)) (Ph_o), 131.2 (t, (J = 29.1 Hz)) (Ph_i), 130.1 (Ph_p), 127.6 (t, (J = 5.4 Hz)) (Ph), 125.3 (HC_{C₅H₄N}), 117.9, 116.9 (HC_{Ar}), 107.6 (C≡ or C_{Ar}), 92.0, 90.5, 69.9, 69.2 (C≡) other quaternary ¹³C were not seen, 31.60, 31.57, 29.3, 29.1, 25.7, 25.4, 22.65, 22.56 (CH₂), 14.1, 14.0 (CH₃) ppm. IR (CH₂Cl₂): 2112 (m) ν(C≡CC₅H₄N); 2102 (s) ν(PtC≡C) cm⁻¹. MS⁺ (MALDI-TOF; m/z): 1524.5 [M]⁺. HR-ESI+-MS: m/z calcd for C₉₀H₉₅N₂O₄P₂¹⁹⁴Pt 1523.6394; found 1523.6362. Anal. Calcd for C₉₀H₉₄N₂O₄P₂Pt: C, 70.89; H, 6.21; N, 1.84. Found: C, 70.72; H, 6.13; N, 1.93. *Crystal data for 1-Pt*: C₉₀H₉₄N₂O₄P₂Pt, M = 1702.93, triclinic, space group P-1, a = 9.5706(4), b = 13.1673(6), c = 16.6608(9) Å, α = 71.273(5), β = 86.786(4), γ = 71.249(4)°, U = 1880.3(2) Å³, F(000) = 788.0, Z = 1, D_c = 1.347 mg m⁻³, μ = 1.962 mm⁻¹; 17913 reflections were collected yielding 8632 unique data (R_{int} = 0.0719). Final wR₂(F²) = 0.1048 for all data (450 refined parameters), conventional R₁(F) = 0.0535 for 7746 reflections with I ≥ 2σ, GOF = 1.007.

Trans-Ru[C≡C{1,4-C₆H₂(OC₆H₁₃)₂}C≡C(4-C₅H₄SMe)]₂(dppe)₂ (**2-Ru**). Compound **3** (40 mg, 0.026 mmol), 4-iodothioanisole (13 mg, 0.052 mmol), Pd(PPh₃)₄ (1.5 mg, 0.001 mmol) and CuI (0.2 mg, 0.001 mmol) were added to a degassed solution of NHⁱPr₂ (5 mL). The yellow solution was heated at 80 °C for 24 h and the precipitate was removed by filtration. The crude solid was purified on a neutral alumina column eluted by CH₂Cl₂/5% NEt₃ to give a yellow powder after removing the solvent. Yield:

1
2
3 15 mg, 34%. ^1H NMR (700 MHz, CD_2Cl_2): δ 7.45 - 7.43 (m, 20H, Ph (16H) +
4 $\text{C}_6\text{H}_4\text{SMe}$ (4H)), 7.23 (d, $J = 7.8$ Hz, 4H, $\text{C}_6\text{H}_4\text{SMe}$), 7.10 (t, $J = 7.4$ Hz, 8H, Ph), 6.92
5 (s, 2H, Ar), 6.88 (t, $J = 7.6$ Hz, 16H, Ph), 5.85 (s, 2H, Ar), 3.92 (t, $J = 6.9$ Hz, 4H,
6 OCH_2), 3.68 (t, $J = 6.4$ Hz, 4H, OCH_2), 2.93 (s, 6H, $\text{C}_6\text{H}_4\text{SMe}$), 1.78 - 1.69 (m, 8H,
7 CH_2), 1.38 - 1.35 (m, 12H, CH_2), 1.26 - 1.20 (m, 12H, CH_2), 0.96 - 0.89 (t, $J = 6.6$
8 Hz, 6H, CH_2CH_3), 0.82 (t, $J = 6.9$ Hz, 6H, CH_3). $^{31}\text{P}\{^1\text{H}\}$ NMR (162 MHz, CDCl_3): δ
9 51.8 (s) ppm. $^{13}\text{C}\{^1\text{H}\}$ NMR (700 MHz, CDCl_3): δ 153.9, 153.3 (O-CAr), 139.1,
10 137.8 (S-CAr), 134.5 (Ph), 131.8 ($\text{HCC}_6\text{H}_4\text{SMe}$), 128.9 (Ph), 127.3, 126.3 (Ph),
11 122.2, 120.9 (CAr), 118.1, 114.8 (HCAr), 106.7, 92.8, 88.2 ($\text{C}\equiv$), 69.41, 69.36
12 (OCH_2), 32.09, 32.07, 30.0, 29.9, 26.2, 23.1, 23.0 (CH_2), 15.7 (SCH_3), 14.3, 14.2
13 (CH_3). MS+ (MALDI-TOF; m/z): 898.1 $[\text{Ru}(\text{dppe})_2]^+$, 1793.3 $[\text{M} + \text{H}]^+$. IR (CH_2Cl_2):
14 2055s $\nu(\text{Ru}-\text{C}\equiv\text{C})$ cm^{-1} . HR-ESI+-MS: calcd for $\text{C}_{110}\text{H}_{118}\text{O}_4\text{P}_4\text{RuS}_2$ 1792.6495;
15 found 1792.6510.
16
17
18
19
20
21
22
23
24
25
26
27
28
29
30
31
32
33
34
35
36

37 *Trans-Pt* $[\text{C}\equiv\text{C}\{1,4\text{-C}_6\text{H}_2(\text{OC}_6\text{H}_{13})_2\}\text{C}\equiv\text{C}(4\text{-C}_5\text{H}_4\text{SMe})]_2(\text{PPh}_3)_2$ (**2-Pt**). Compound
38 **6** (90 mg, 0.064 mmol), 4-iodothioanisole (37.5 mg, 0.15 mmol), $\text{Pd}(\text{PPh}_3)_4$ (4 mg,
39 0.003 mmol) and CuI (1 mg) were added to a Schlenk flask charged with degassed
40 HN^iPr_2 (8 mL), and the reaction mixture was heated for 2 h at 100 °C. The yellow
41 solution was evaporated to dryness and the residue was purified on a silica column
42 eluted by CH_2Cl_2 :hexane (1 : 1 v/v) followed by pure CH_2Cl_2 to give yellow crystals.
43 Yield: 17 mg, 17%. X-ray quality crystals were grown by slow diffusion of methanol
44 into a solution of the complex in 95:5 CH_2Cl_2 / NEt_3 (v:v). ^1H NMR (600 MHz,
45 CDCl_3) : δ 7.84 - 7.81 (m, 12H, Ph), 7.38 (d, $J = 9.1$ Hz, 4H, $\text{C}_6\text{H}_4\text{SMe}$), 7.33 - 7.27
46 (m, 18H, Ph), 7.17 (d, $J = 9.1$ Hz, 4H, $\text{C}_6\text{H}_4\text{SMe}$), 6.68 (s, 2H, Ar), 5.77 (s, 2H, Ar),
47 3.78 (t, $J = 6.5$ Hz, 4H, O- CH_2), 3.54 (t, $J = 6.9$ Hz, 4H, OCH_2), 2.48 (s, 6H, SCH_3),
48
49
50
51
52
53
54
55
56
57
58
59
60

1
2
3 1.76 - 1.71 (m, 4H, CH₂), 1.51 - 1.47 (m, 4H, CH₂), 1.36 - 1.27 (m, 16H, CH₂), 1.21 -
4
5 1.14 (m, 8H, CH₂), 0.91 - 0.86 (m, 12H, CH₂CH₃) ppm. ³¹P{¹H} NMR (162 MHz,
6
7 CDCl₃): δ 17.6 (s, J_{P-Pt} = 2653.1 Hz) ppm. ¹³C{¹H} NMR (101 MHz, CDCl₃): δ
8
9 153.3, 152.5 (OCAr), 138.4 (S-CAr), 135.3 (t, J = 6.2 Hz, Ph), 131.6 (HCC₆H₄SMe),
10
11 131.3 (t, J = 29.2 Hz, Ph), 130.1 (Ph), 127.6 (t, J = 5.5 Hz, Ph), 125.9 (HCC₆H₄SMe),
12
13 120.7, 120.5 (CAr), 117.7, 117.2 (HCAr), 109.1, 92.9, 86.9 (C≡), 69.8, 69.2 (OCH₂),
14
15 31.64, 31.58, 29.4, 29.1, 25.8, 25.5, 22.7, 22.6 (CH₂), 15.5 (SCH₃), 14.12, 14.08
16
17 (CH₃) ppm. MS⁺ (MALDI-TOF; m/z): 719.4 [Pt(PPh₃)₂]⁺, 1614.3 [M + H]⁺. IR
18
19 (CH₂Cl₂): ν(Pt-C≡C) 2104 (s) cm⁻¹. HR-(ESI⁺)-MS: calcd for C₉₄H₁₀₀O₄P₂PtS₂Na
20
21 1637.6107; found 1637.6124. *Crystal data for 2-Pt*: C₉₄H₁₀₀O₄P₂PtS₂, M = 1614.89,
22
23 monoclinic, space group P2/n, a = 22.659(10), b = 9.469(4), c = 22.765(10) Å, β =
24
25 118.005(5)°, U = 4313(3) Å³, F(000) = 1672.0, Z = 2, D_c = 1.622 mg m⁻³, μ = 1.244
26
27 mm⁻¹, crystal size 0.01 x 0.01 x 0.001 mm³; 42922 reflections were collected yielding
28
29 8352 unique data (R_{int} = 0.2997). Final wR₂(F²) = 0.2517 for all data (371 refined
30
31 parameters), conventional R₁(F) = 0.0949 for 4614 reflections with I ≥ 2σ, GOF =
32
33 1.024.
34
35
36
37
38
39
40
41
42
43
44
45

46 *Single molecule conductance measurements*

47
48 Gold on glass substrates (Arrandee, Schröer, Germany) were cleaned with acetone
49
50 and flame-annealed with a butane torch until a slight orange hue was obtained. The
51
52 slide was kept in this state for 20 seconds during which time the torch was kept in
53
54 motion around the sample to avoid overheating. This procedure was performed three
55
56 times to generate flat Au (111) terraces.⁶⁵ The freshly-annealed substrates were
57
58 immersed in a 10⁻⁴ M acetonitrile (99.9% ChromasolV Plus for HPLC) solution of the
59
60

1
2
3 complex under investigation for 1 minute, after which time the gold sample was
4 removed and washed with ethanol and then dried in an argon flow. The short
5 immersion time and low concentration of solution were chosen to promote low
6 molecular coverage of the gold surface, which increases the formation of single
7 molecule events over aggregate phenomena.
8
9

10
11
12
13
14
15
16
17 Conductance values of the compounds and the break-off distances were obtained with
18 a STM (Agilent 5500 SPM microscope), using the $I(s)$ technique in which an
19 electrochemically-etched gold tip is approached close to the substrate surface and then
20 retracted with the tunneling current (I) recorded against distance (s).⁴⁸ The Agilent
21 5500 SPM was fitted with a low-current preamplifier and set point conditions of $I =$
22 30 nA and bias voltage, $U_{tip} = 0.6$ V were employed. The $I(s)$ method involves
23 repeatedly moving the STM tip towards the gold surface to given set-point values and
24 then rapidly away from the surface. During these cycles molecular junctions are
25 occasionally formed which can be recognized by deviations from the usual
26 exponential decay of current in the form of current plateaus. In this case as the
27 junction is stretched beyond its maximum length, the molecular bridge breaks, leading
28 to a sharp decrease in current and currents steps. Hence these junction formation and
29 cleavage processes are recognized by plateaus and steps in the current-distance
30 currents. Since the $I(s)$ technique is a “non-contact” method (no metallic contact
31 between the gold STM tip and gold surface) the molecular junction formation
32 probability, as recognized by the plateau-step traces, is significantly smaller than for
33 break junction techniques. The $I(s)$ tip retraction cycles are repeated many times
34 (normally 4000-5000 traces) in order to record sufficient traces where molecular
35 junctions form, called molecular junction formation scans, as opposed to most traces
36
37
38
39
40
41
42
43
44
45
46
47
48
49
50
51
52
53
54
55
56
57
58
59
60

1
2
3 for which no junction forms. Molecular junction formation scans are recognized by
4 recording only traces which exhibit a plateau longer than 1 Å, present in about 15% of
5
6 all traces for both anchor groups. The resulting $I(s)$ curves are binned in current steps
7
8 (16 pS) and plotted to give a conductance histogram comprised of at least 500 $I(s)$
9
10 scans showing plateaus. The error associated with each current value reported has
11
12 been statistically obtained from the standard deviation of the points comprising the
13
14 conductance peak.
15
16
17
18
19
20
21

22 *Single-crystal X-ray crystallography*

23
24 The X-ray single crystal data for crystal **1-Ru** have been collected using λ MoK α
25 radiation ($\lambda = 0.71073 \text{ \AA}$) on a Bruker D8Venture (Photon100 CMOS detector, I μ S-
26
27 microsource, focusing mirrors) and for crystal **1-Pt** on an Agilent XCalibur
28
29 (Sapphire-3 CCD detector, fine-focus sealed tube, graphite monochromator)
30
31 diffractometers equipped with a Cryostream (Oxford Cryosystems) open-flow
32
33 nitrogen cryostats at the temperature 120.0(2)K. The data for extremely small and
34
35 weakly diffracting crystals **2-Pt** were collected at 100.0(2)K on a Rigaku Saturn 724+
36
37 diffractometer at station I19 of the Diamond Light Source (UK) synchrotron
38
39 (undulator, $\lambda = 0.6889 \text{ \AA}$, ω -scan, 1.0°/frame) and processed using Bruker APEXII
40
41 software. All structures were solved by direct method and refined by full-matrix least
42
43 squares on F^2 for all data using Olex2⁶⁶ and SHELXTL⁶⁷ software. All non-
44
45 disordered non-hydrogen atoms were refined anisotropically, the hydrogen atoms
46
47 were placed in the calculated positions and refined in riding mode. Disordered atoms
48
49 in structure **2-Pt** were refined isotropically with fixed SOF=0.6 and 0.4. The structure
50
51 **2-Pt** also contains severely disordered solvent molecules (probably DCM) which
52
53 could not be reliably identified and modelled properly. Their contribution to the
54
55
56
57
58
59
60

1
2
3 structural factors was taken into account by applying MASK procedure of Olex2
4 program package. Crystallographic data for the structure have been deposited with the
5
6 Cambridge Crystallographic Data Centre as supplementary publication CCDC-
7
8 1483157-1483159.
9
10
11

12 13 14 15 16 17 18 *Theoretical methods*

19
20 Gas-phase optimizations were performed with the Gaussian 09 program package,⁶⁸
21
22 using the B3LYP functional⁵⁰ and LANL2DZ basis set on Ru and Pt⁵¹ and 6-31G**
23
24 on all other atoms.⁵² Results were further analyzed using the GaussSum package.⁶⁹
25
26
27

28
29 The DFT-Landauer approach used in the modeling of molecular junctions assumes
30
31 that on the timescale taken by an electron to traverse the molecule, inelastic scattering
32
33 is negligible. This is known to be an accurate assumption for molecules up to several
34
35 nm in length.⁵⁷ All molecules in this work have been relaxed in isolation. Geometry
36
37 optimizations were carried out using the DFT code SIESTA, with a generalized
38
39 gradient approximation (PBE functional),⁷⁰ double- ζ polarized basis set, 0.01 eV/Å
40
41 force tolerance and a real-space grid with a plane wave cut-off energy of 250 Ry, zero
42
43 bias voltage and 1 k points.
44
45
46
47
48
49

50
51 To compute the electrical conductance, the molecules were then placed in the vicinity
52
53 of the metal | molecule | metal junctions. Each molecule has been attached to two
54
55 (111) directed gold electrodes; one of these electrodes is pyramidal, while the other
56
57 one is a planar electrode, then the molecules and the first layer of electrodes were
58
59 allowed to relax again, yielding the optimal junctions geometries as shown in Figure
60

1
2
3
4
5
6
7
8
9
10
11
12
13
14
15
16
17
18
19
20
21
22
23
24
25
26
27
28
29
30
31
32
33
34
35
36
37
38
39
40
41
42
43
44
45
46
47
48
49
50
51
52
53
54
55
56
57
58
59
60

7. These layers were then used to extend the gold electrodes to infinity. For each structure, the transmission coefficient $T(E)$ describing the propagation of electrons of energy E from the left to the right electrode was calculated by first obtaining the corresponding Hamiltonian and overlap matrices using SIESTA and then using the GOLLUM code to compute $T(E)$ via the relation $T(E) = \text{Tr}\{\Gamma_R(E)G^R(E)\Gamma_L(E)G^{R\dagger}(E)\}$, in this expression, $\Gamma_{L,R}(E) = i\left(\Sigma_{L,R}(E) - \Sigma_{L,R}^\dagger(E)\right)$ describes the level broadening due to the coupling between left (L) and right (R) electrodes and the central scattering region, $\Sigma_{L,R}(E)$ are the retarded self-energies associated with this coupling and $G^R = (ES - H - \Sigma_L - \Sigma_R)^{-1}$ is the retarded Green's function, where H is the Hamiltonian and S is the overlap matrix (both of them obtained from SIESTA). Finally the room temperature electrical conductance G was computed from the formula $G = G_0 \int_{-\infty}^{\infty} dE T(E) \left(-\frac{df(E)}{dE}\right)$ where $f(E) = [e^{\beta(E-E_F)} + 1]^{-1}$ is the Fermi function, $\beta=1/k_B T$, E_F is the Fermi energy and $G_0 = \left(\frac{2e^2}{h}\right)$ is the quantum of conductance. Since the quantity $\left(-\frac{df(E)}{dE}\right)$ is a probability distribution peaked at $E = E_F$, with a width of the order $k_B T$, the above expression shows that G/G_0 is obtained by averaging $T(E)$ over an energy range of order $k_B T$ in the vicinity of $E=E_F$. It is well-known that the Fermi energy E_F^{DFT} predicted by DFT is not usually reliable and therefore plots are shown of G/G_0 as a function of $E_F - E_F^{\text{DFT}}$. To determine E_F , we compared the predicted values of all molecules with the experimental values and chose a single common value of E_F which gave the closest overall agreement. This yielded a value of $E_F - E_F^{\text{DFT}} = -0.07$ eV, which is used in all theoretical results.

1
2
3
4
5
6
7 ASSOCIATED CONTENT
89
10 **Supporting Information.**
11

12
13 The Supporting Information is available free of charge at the ACS Publications
14 website at DOI...
15
16

17
18
19 Crystallographic data in .cif format.
20

21
22 A text file of all computed molecule Cartesian coordinates in .xyz format for
23 convenient visualization
24
25
26
27
28
29
30
31
32

33 AUTHOR INFORMATION
3435 **Corresponding Authors**
36

37
38 *E-mail: c.lambert@lancaster.ac.uk.
39

40 *E-mail: paul.low@uwa.edu.au.
41

42 *E-mail: nichols@liv.ac.uk.
43

44 *E-mail: m.r.bryce@durham.ac.uk
45

46 AUTHOR CONTRIBUTIONS
47

48
49 Θ These authors contributed equally to this work.
50
51
52

53
54 **Notes**
55

56
57 The authors declare no competing financial interest.
58
59
60

Acknowledgements

C.J.L. and O.A.A. acknowledge financial support from the Ministry of Higher Education and Scientific Research of Iraq. C.J.L. and M.R.B. acknowledge funding from the EU through the FP7 ITN MOLESCO (project number 212942). P.J.L. holds an ARC Future Fellowship (FT120100073) and gratefully acknowledges funding for this work from the ARC (DP140100855). S.B. holds an International Postgraduate Research Scholarship and gratefully acknowledges support from the University of Western Australia. R.J.N. and S.J.H. thank EPSRC for funding (grant EP/H035184/1 and EP/K007785/1). We thank the Diamond Light Source for an award of instrument time on the Station I19 (MT 6749) and the instrument scientists for support.

References

1. Zhang, J.; Kuznetsov, A.M.; Medvedev, I.G.; Chi, Q.; Albrecht, T.; Jensen, P.S.; Ulstrup, J. *Chem. Rev.* **2008**, *108*, 2737-2791
2. Nichols, R.J.; Haiss, W.; Higgins, S.J.; Leary, E.; Martin, S.; Bethell, D. *Phys. Chem. Chem. Phys.* **2010**, *12*, 2801.
3. Kiguchi, M.; Kaneko, S. *Phys. Chem. Chem. Phys.* **2013**, *15*, 2253
4. Low, P.J. *Dalton Trans.* **2005**, 2821-2824
5. Rigaut, S. *Dalton Trans.* **2013**, *42*, 15859-15863
6. Park, J.; Pasupathy, A.N.; Goldsmith, J.I.; Chang, C.; Yaish, Y.; Petta, J.R.; Rinkoski, M.; Sethna, J.P.; Abruna, H.D.; McEuen, P.L.; Ralph, D.C. *Nature*, **2002**, *417*, 722-725
7. Liang, W.J.; Shores, M.P.; Bockrath, M.; Long, J.R.; Park, H. *Nature*, **2002**, *417*, 725-729.

- 1
2
3
4
5
6
7
8
9
10
11
12
13
14
15
16
17
18
19
20
21
22
23
24
25
26
27
28
29
30
31
32
33
34
35
36
37
38
39
40
41
42
43
44
45
46
47
48
49
50
51
52
53
54
55
56
57
58
59
60
8. Albrecht, T.; Moth-Poulsen, K.; Christensen, J.B.; Guckian, A.; Bjornholm, T.; Vos, J.G.; Ulstrup, J. *Faraday Diss.* **2006**, *131*, 265-279.
 9. Ricci, A.M.; Calvo, E.J.; Martin, S.; Nichols, R.J. *J. Am. Chem. Soc.*, **2010**, *132*, 2494-2495.
 10. Ponce, J.; Arroyo, C.R.; Tatay, S.; Frisenda, R.; Gaviña, P.; Aravena, D.; Ruiz, E.; van der Zant, H.S.J.; Coronado, E. *J. Am. Chem. Soc.*, **2014**, *136*, 8312.
 11. Li, J.-C.; Wu, J.-Z.; Gong, Z. *J. Phys., Chem. Lett.* **2014**, *5*, 1017-1021.
 12. Sakamoto, R.; Katagiri, S.; Maeda, H.; Nishihara, H. *Coord. Chem. Rev.* **2013**, *257*, 1493-1506.
 13. Davidson, R.; Liang, J.H.; Milan, D.C.; Mao, B.-W.; Nichols, R.J.; Higgins, S.J.; Yufit, D.S.; Beeby, A.; Low, P.J. *Inorg. Chem.* **2015**, *54*, 5487-5494.
 14. Aragonès, A.C.; Aravena, D.; J.I.; Acís-Castillo, Z.; Li, H.; Real, J. A.; Sanz, F.; Hihath, J.; Ruiz, E.; Díez-Pérez, I. *Nano Lett.*, **2016**, *16*, 218-226.
 15. Zotti, L.A.; Leary, E.; Soriano, M.; Cuevas, J.C.; Palacios, J.J. *J. Am. Chem. Soc.* **2013**, *135*, 2052-2055.
 16. Leary, E.; Van Zalinge, H.; Higgins, S.J.; Nichols, R.J.; de Biani, F.F.; Leoni, P.; Marchetti, L.; Zanello, P. *Phys. Chem. Chem. Phys.* **2009**, *11*, 5198-5202.
 17. Choi, B.; Capozzi, B.; Ahn, S.; Turkiewicz, A.; Lovat, G.; Nuckolls, C.; Steigerwald, M.L.; Venkataraman, L.; Roy, X. *Chem. Sci.*, **2016**, *7*, 2710-2705.
 18. Zotti, L.A.; Leary, E.; Soriano, M.; Cuevas, J.C.; Palacios, J.J. *J. Am. Chem. Soc.* **2013**, *135*, 2052-2055.
 19. Wang, W.Z.; Wu, Y.; Ismayilov, R.H.; Juo, J.H.; Yeh, C.Y.; Lee, H.W.; Fu, M.D.; Chen, C.H.; Lee, G.H.; Peng, S.M. *Dalton Trans.* **2014**, *43*, 6229-6235.

- 1
2
3
4
5
6
7
8
9
10
11
12
13
14
15
16
17
18
19
20
21
22
23
24
25
26
27
28
29
30
31
32
33
34
35
36
37
38
39
40
41
42
43
44
45
46
47
48
49
50
51
52
53
54
55
56
57
58
59
60
20. Tsai, C.S.; Liu, I.P.C.; Tien, F.W.; Lee, G.H.; Yeh, C.Y.; Chen, C.H.; Peng, S.M. *Inorg. Chem. Commun.* **2013**, *38*, 152-155.
21. Chen, I.W.P.; Fu, M.D.; Tseng, W.H.; Yu, J.Y.; Wu, S.H.; Ku, C.J.; Chen, C.H.; Peng, S.M. *Angew. Chem. Int. Ed.* **2006**, *45*, 5814-5818.
22. Mayor, M.; von Hanisch, C.; Weber, H.B.; Reichert, J.; Beckmann, D. *Angew. Chem. Int. Ed.* **2002**, *41*, 1183-1186.
23. Schull, T.L.; Kushmerick, J.G.; Patterson, C.H.; George, C.; Moore, M.H.; Pollack, S.K.; Shashidhar, R. *J. Am. Chem. Soc.* **2003**, *125*, 3202-3203.
24. Mahapatro, A.K.; Ying, J.W.; Ren, T.; Janes, D.B. *Nano Lett.* **2008**, *8*, 2131-2136.
25. Schwarz, F.; Kastlunger, G.; Lissel, F.; Egler-Lucas, C.; Semenov, S.N.; Venkatesan, K.; Berke, H.; Stadler, R.; Lortscher, E. *Nature Nanotech.* **2016**, *11*, 170-177.
26. Schwarz, F.; Kastlunger, G.; Lissel, F.; Riel, H.; Venkatesan, K.; Berke, H.; Stadler, R.; Lortscher, E. *Nano Lett.* **2014**, *14*, 5932-5940.
27. Lissel, F.; Schwarz, F.; Blacque, O.; Riel, H.; Lortscher, E.; Venkatesan, K.; Berke, H. *J. Am. Chem. Soc.* **2014**, *136*, 14560-14569.
28. Sugimoto, K.; Tanaka, Y.; Fujii, S.; Tada, T.; Kiguchi, M.; Akita, M. *Chem. Commun.* **2016**, *52*, 5796-5799.
29. Marques-Gonzalez, S.; Yufit, D.S.; Howard, J.A.K.; Martin, S.; Osorio, H.M.; Garcia-Suarez, V.M.; Nichols, R.J.; Higgins, S.J.; Cea, P.; Low, P.J. *Dalton Trans.* **2013**, *42*, 338-341.
30. Meng, F.B.; Hervault, Y.M.; Shai, Q.; Hu, B.H.; Norel, L.; Rigaut, S.; Chen, X.D. *Nature Commun.* **2014**, *5*, 3023.

- 1
2
3
4
5
6
7
8
9
10
11
12
13
14
15
16
17
18
19
20
21
22
23
24
25
26
27
28
29
30
31
32
33
34
35
36
37
38
39
40
41
42
43
44
45
46
47
48
49
50
51
52
53
54
55
56
57
58
59
60
31. Luo, L.; Benameur, A.; Brignou, P.; Choi, S.H.; Rigaut, S.; Frisbie, C.D. *J. Phys. Chem. C* **2011**, *115*, 19955-19961.
32. Kim, B.; Beebe, J.M.; Olivier, C.; Rigaut, S.; Touchard, D.; Kushmerick, J.G.; Zhu, X.Y.; Frisbie, C.D. *J. Phys. Chem. C* **2007**, *111*, 7521-7526.
33. Wen, H.-M.; Yang, Y.; Zhou, X.-S.; Liu, J.-Y.; Zhang, D.-B.; Wang, J.-Y.; Chen, Z.-N.; Tian, Z.-Q.; *Chem. Sci.*, **2013**, *4*, 2471-2477.
34. Liu, K.; Wang, X.H.; Wang, F.S. *ACS Nano*, **2008**, *2*, 2315-2323.
35. Zhao, X.T.; Huang, C.; Gulcur, M.; Batsanov, A.S.; Baghernejad, M.; Hong, W.; Bryce, M.R.; Wandlowski, T. *Chem. Mater.* **2013**, *25*, 4340-4347.
36. Schull, T.L.; Kushmerick, J.G.; Paterson, C.H.; George, C.; Moore, M.H.; Pollack, S.K.; Shashidhar, R. *J. Am. Chem. Soc.* **2003**, *125*, 3202-3203.
37. Hong, W.; Manrique, D.Z.; Moreno-García, P.; Gulcur, M.; Mishchenko, A.; Lambert, C.J.; Bryce, M.R.; Wandlowski, T. *J. Am. Chem. Soc.* **2012**, *134*, 2292-2304.
38. Martin, S.; Grace, I.; Bryce, M.R.; Wang, C.S.; Jitchati, R.; Batsanov, A.S.; Higgins, S.J.; Lambert, C.J.; Nichols, R.J. *J. Am. Chem. Soc.* **2010**, *132*, 9157-9164.
39. Park, Y.S.; Whalley, A.C.; Kamenetska, M.; Steigerwald, M.L.; Hybertsen, M.S.; Nuckolls, C.; Venkataraman, L. *J. Am. Chem. Soc.* **2007**, *129*, 15768-15769.
40. Kamenetska, M.; Quek, S.Y.; Whalley, A.C.; Steigerwald, M.L.; Choi, H.J.; Louie, S.G.; Nuckolls, C.; Hybertsen, M.S.; Neaton, J.B.; Venkataraman, L. *J. Am. Chem. Soc.*, **2010**, *132*, 6817-6821.
41. Kirn, T.; Vazquez, H.; Hybertsen, M.S.; Venkataraman, L. *Nano Lett.* **2013**, *13*, 3358-3364.

- 1
2
3
4
5
6
7
8
9
10
11
12
13
14
15
16
17
18
19
20
21
22
23
24
25
26
27
28
29
30
31
32
33
34
35
36
37
38
39
40
41
42
43
44
45
46
47
48
49
50
51
52
53
54
55
56
57
58
59
60
42. Saitner, M.; Eberle, F.; Baccus, J.; D'Olieslaeger, M.; Wagner, P.; Kolb, D.M.; Boyen, H.-G. *J. Phys. Chem. C* **2012**, *116*, 21810-21815.
43. Davidson, R.; Al-Owaedi, O.A.; Milan, D.C.; Zeng, Q.; Tory, J.; Hartl, F.; Higgins, S.J.; Nichols, R.J.; Lambert, C.J.; Low, P.J. *Inorg. Chem.* **2016**, *55*, 2691-2700.
44. Ricci, A.M.; Calvo, E.J.; Martin, S.; Nichols, R.J. *J. Am. Chem. Soc.* **2010**, *132*, 2494-2495.
45. Ballesteros, L.M.; Martín, S.; Marques-Gonzalez, S.; Lopez, M.C.; Higgins, S.J.; Nichols, R.J.; Low, P.J.; Cea, P. *J. Phys. Chem. C* **2015**, *119*, 784-793.
46. Wang, C.; Batsanov, A.S.; Bryce, M.R.; Martin, S.; Nichols, R.J.; Higgins, S.J.; Garcia-Suarez, V.M.; Lambert, C.J. *J. Am. Chem. Soc.* **2009**, *131*, 15647-15654.
47. Moreno-Garcia, P.; Gulcur, M.; Manrique, D.Z.; Pope, T.; Hong, W.J.; Kaliginedi, V.; Huang, C.C.; Batsanov, A.S.; Bryce, M.R.; Lambert, C.; Wandlowski, T. *J. Am. Chem. Soc.* **2013**, *135*, 12228-12240.
48. Haiss, W.; van Zalinge, H.; Higgins, S.J.; Bethell, D.; Hobenreich, H.; Schiffrin, D.J.; Nichols, R.J. *J. Am. Chem. Soc.* **2003**, *125*, 15294-15295.
49. Capozzi, B.; Dell, E.J.; Berkelbach, T.C.; Reichman, D.R.; Venkataraman, L.; Campos, L.M. *J. Am. Chem. Soc.* **2014**, *136*, 10486-10492
50. (a) Becke, A.D. *J. Chem. Phys.* **1993**, *98*, 5648-5652. (b) Stephens, P.J.; Devlin, F.J.; Chabalowski, C.F.; Frisch, M.J. *J. Phys. Chem.* **1994**, *98*, 11623-11627.
51. (a) Hay, P.J.; Wadt, W.R. *J. Chem. Phys.* **1985**, *82*, 270-283. (b) Wadt, W.R.; Hay, P.J. *J. Chem. Phys.* **1985**, *82*, 284-298. (c) Hay, P.J.; Wadt, W.R. *J. Chem. Phys.* **1985**, *82*, 299-310.

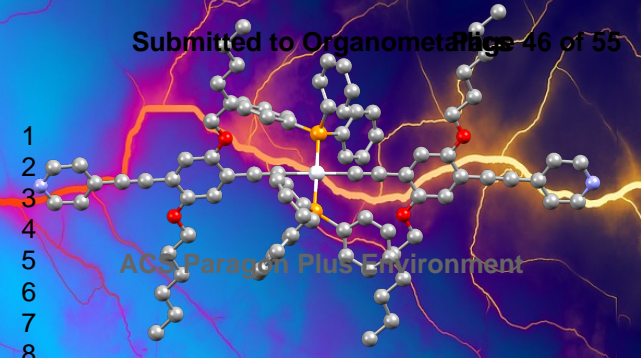
- 1
2
3
4 52. (a) Petersson, G.A.; Bennett, A.; Tensfeldt, T.G.; Al-Laham, M.A.; Shirley,
5
6 W.A.; Mantzaris, J. *J. Chem. Phys.* **1998**, *89*, 2193-2198. (b) Petersson, G.A.;
7
8 Al-Laham, M.A. *J. Chem. Phys.* **1991**, *94*, 6081-6090.
9
10 53. Marques-Gonzalez, S.; Parthey, M.; Yufit, D.S.; Howard, J.A.K.; Kaupp, M.;
11
12 Low, P.J. *Organometallics* **2014**, *33*, 4947-4963.
13
14 54. Georgiev, V.P.; McGrady, J.E. *J. Am. Chem. Soc.* **2011**, *133*, 12590-12599.
15
16 55. Ferrer, J.; Lambert, C.J.; Garcia-Suarez, V.M.; Manrique, D.Z.; Visontai, D.;
17
18 Oroszlany, L.; Rodriguez-Ferradas, R.; Grace, I.; Bailey, S.W.D.; Gillemot,
19
20 K.; Sadeghi, H.; Algharagholy, L. *New J. Phys.* **2014**, *16*, 093029.
21
22 56. Lambert, C.J. *Chem. Soc. Rev.* **2015**, *44*, 875-888.
23
24 57. Markussen, T.; Settnes, M.; Thygesen, K.S. *J. Chem. Phys.* **2011**, *135*, 144104
25
26 58. Häkkinen, H. *Nature Chem.* **2012**, *4*, 443-455.
27
28 59. Mishchenko, A.; Zotti, L.A.; Vonlanthen, D.; Burkle, M.; Pauly, F.; Cuevas,
29
30 J.C.; Mayor, M.; Wandlowski, T. *J. Am. Chem. Soc.* **2011**, *133*, 184-187.
31
32 60. Quek, S.Y.; Kamenetska, M.; Steigerwald, M.L.; Choi, H.J.; Louie, S.G.;
33
34 Hybertsen, M.S.; Neaton, J.B.; Venkataraman, L. *Nat. Nanotechnol.* **2009**, *4*,
35
36 230-234.
37
38 61. Dell, E.J.; Capozzi, B.; Xia, J.L.; Venkataraman, L.; Campos, L.M. *Nature*
39
40 *Chem.* **2015**, *7*, 209-214.
41
42 62. Fox, M.A.; Harris, J.E.; Heider, S.; Pérez-Gregorio, V.; Zakrzewska, M.E.;
43
44 Farmer, J.D.; Yufit, D.S.; Howard, J.A.K.; Low, P.J. *J. Organomet. Chem.*
45
46 **2009**, *694*, 2350-2358.
47
48 63. Bailar, J.C. Jr.; Itatani, H. *Inorg. Chem.* **1965**, *4*, 1618-1620.
49
50 64. Zhou, C.-Z.; Liu, T.; Xu, J.-M.; Chen, Z.-K. *Macromolecules*, **2003**, *36*, 1457-
51
52 1464.
53
54
55
56
57
58
59
60

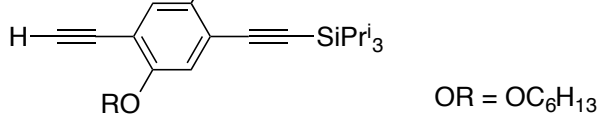
- 1
2
3
4
5
6
7
8
9
10
11
12
13
14
15
16
17
18
19
20
21
22
23
24
25
26
27
28
29
30
31
32
33
34
35
36
37
38
39
40
41
42
43
44
45
46
47
48
49
50
51
52
53
54
55
56
57
58
59
60
65. Haiss, W.; Lackey, D.; Sass, J. K.; Besocke, K. H. *J. Chem. Phys.* **1991**, *95*, 2193-2196.
66. Dolomanov, O.V., Bourhis, L.J., Gildea, R.J., Howard, J. A. K., Puschmann, H. *J. Appl. Cryst.* **2009**, *42*, 339-341.
67. Sheldrick, G.M. *Acta Cryst.* **2008**, *A64*, 112-122.
68. Frisch, M.J.; Trucks, G.W.; Schlegel, H.B.; Scuseria, G.E.; Robb, M.A.; Cheeseman, J.R.; Scalmani, G.; Barone, V.; Mennucci, B.; Petersson, G.A.; Nakatsuji, H.; Caricato, M.; Li, X.; Hratchian, H.P.; Izmaylov, A.F.; Bloino, J.; Zheng, G.; Sonnenberg, J.L.; Hada, M.; Ehara, M.; Toyota, K.; Fukuda, R.; Hasegawa, J.; Ishida, M.; Nakajima, T.; Honda, Y.; Kitao, O.; Nakai, H.; Vreven, T.; Montgomery, J. A.; Peralta, J.E.; Ogliaro, F.; Bearpark, M.; Heyd, J.J.; Brothers, E.; Kudin, K.N.; Staroverov, V. N.; Kobayashi, R.; Normand, J.; Raghavachari, K.; Rendell, A.; Burant, J.C.; Iyengar, S.S.; Tomasi, J.; Cossi, M.; Rega, N.; Millam, J.M.; Klene, M.; Knox, J.E.; Cross, J.B.; Bakken, V.; Adamo, C.; Jaramillo, J.; Gomperts, R.; Stratmann, R.E.; Yazyev, O.; Austin, A. J.; Cammi, R.; Pomelli, C.; Ochterski, J. W.; Martin, R. L.; Morokuma, K.; Zakrzewski, V.G.; Voth, G.A.; Salvador, P.; Dannenberg, J. J.; Dapprich, S.; Daniels, A. D.; Farkas, Ö.; Foresman, J.B.; Ortiz, J.V.; Cioslowski, J.; Fox, D.J. *Gaussian 09, Revision D.01*; Gaussian Inc.: Wallingford, CT, 2009.
69. O'Boyle, N.M.; Tenderholt, A.L.; Langner, K.M. *J. Comput. Chem.* **2008**, *29*, 839-845.
70. Perdew, J.P.; Chevary, J.A.; Vosko, S.H.; Kackson, K.A.; Pederson, M.R.; Singh, D.J.; Fiolhais, C. *Phys. Rev. B*, **1992**, *46*, 6671-6687.

Submitted to Organometallics 46 of 55

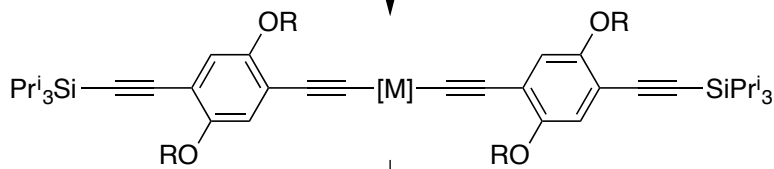
1
2
3
4
5
6
7
8

ACS Paragon Plus Environment

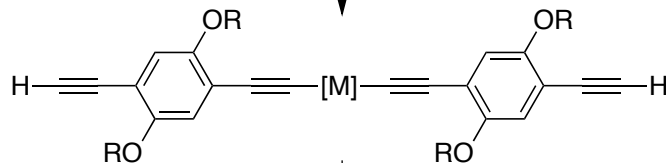




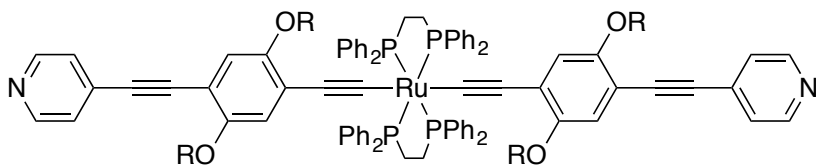
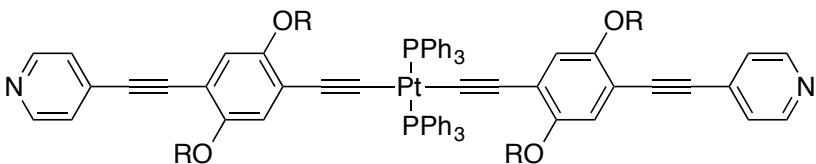
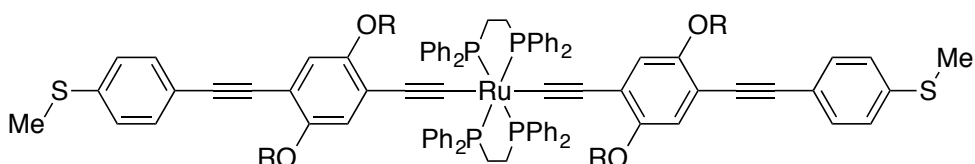
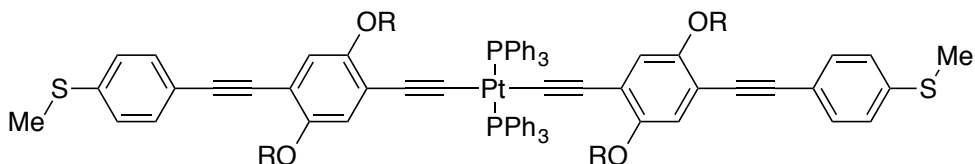
(i)

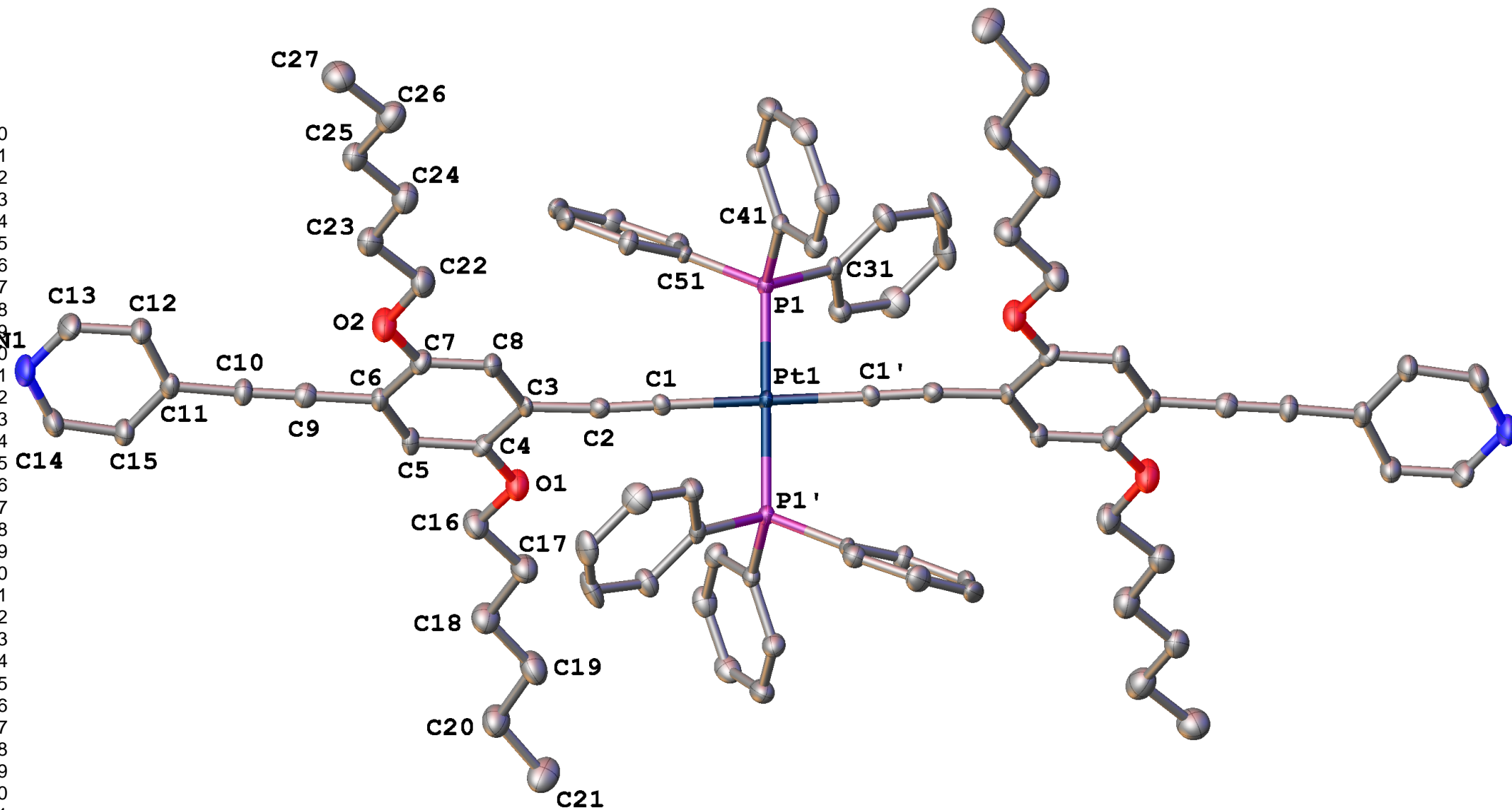


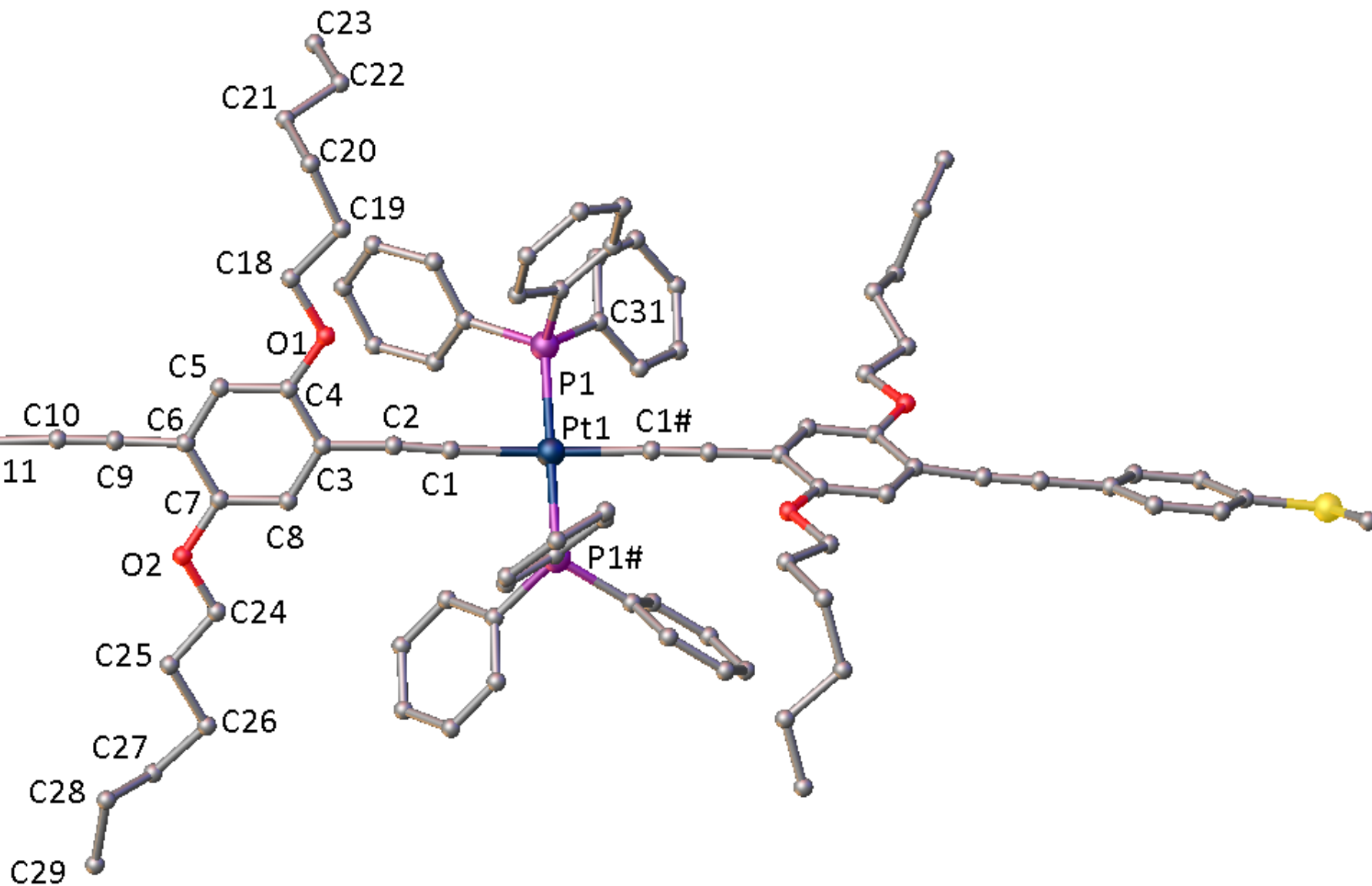
(ii)

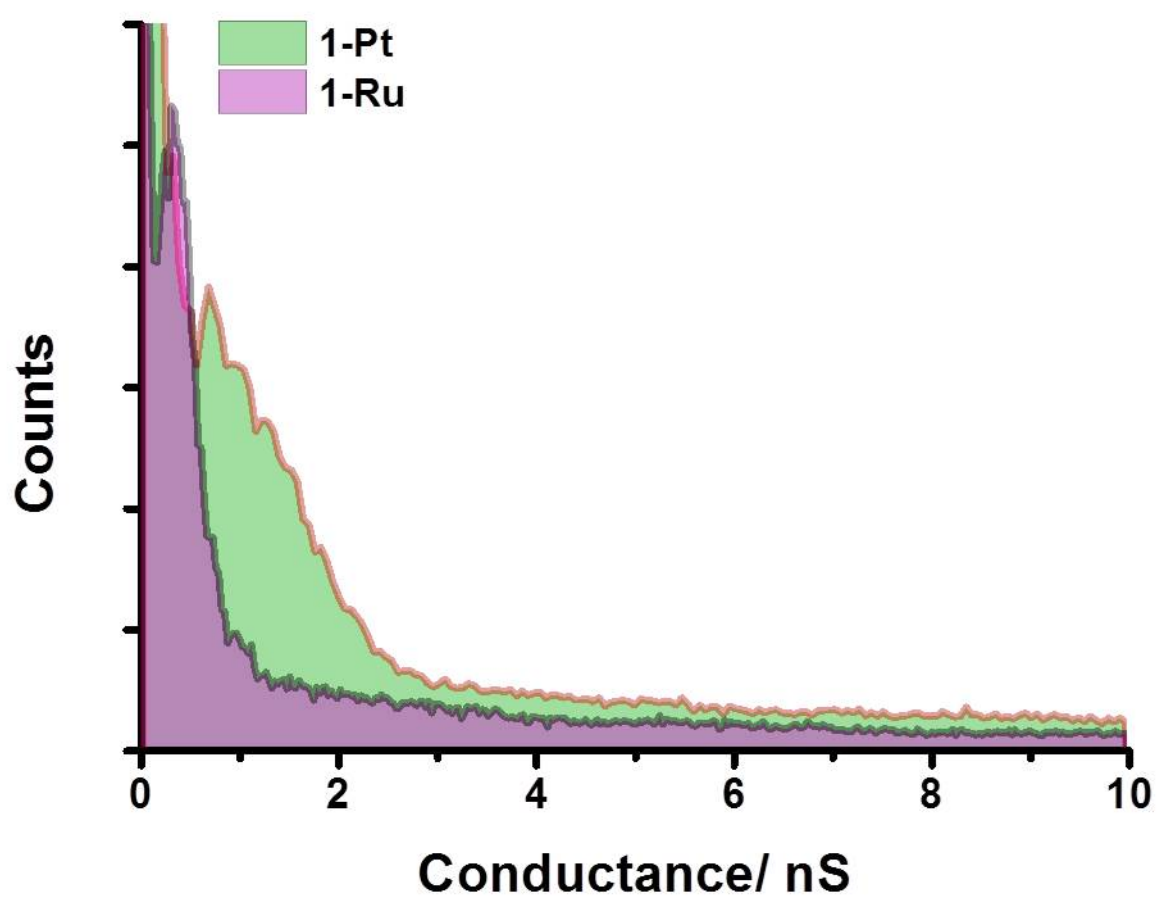


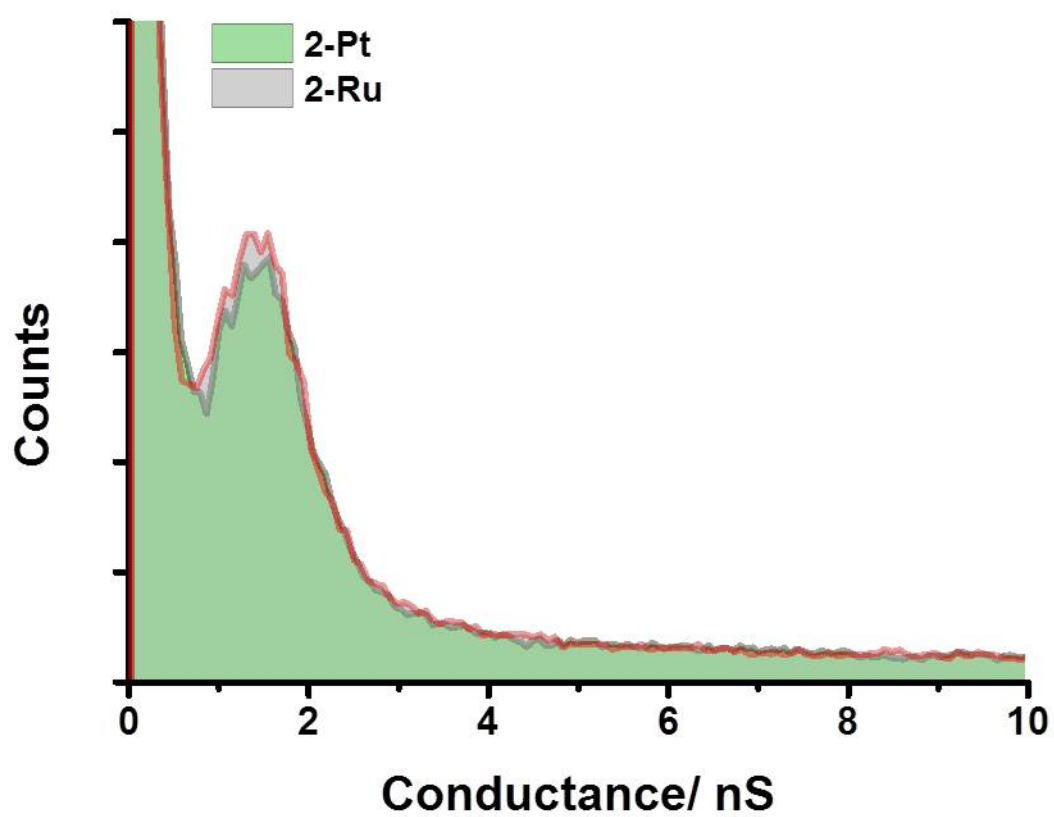
(iii)

1-Ru, 1-Pt, 2-Ru, 2-Pt**1-Ru****1-Pt****2-Ru****2-Pt**

1
2
3
4
5
6
7
8
9
10
11
12
13
14
15
16
17
18
19
20
21
22
23
24
25
26
27
28
29
30
31
32
33
34
35
36
37
38
39
40
41
42
43
44
45
46
47

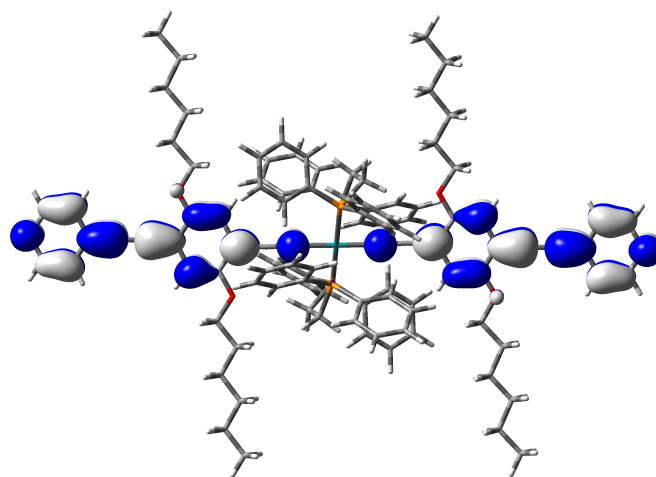
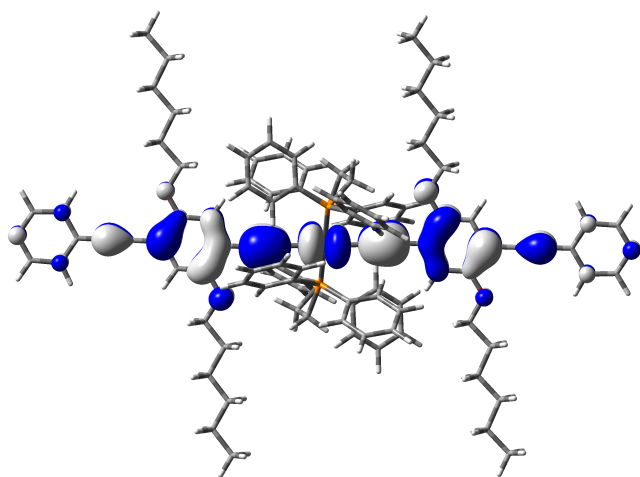
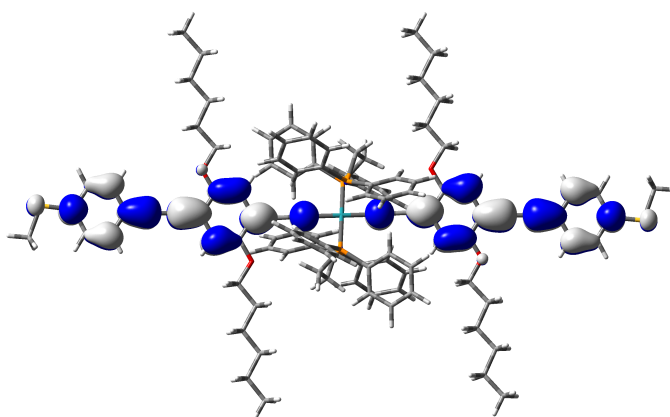
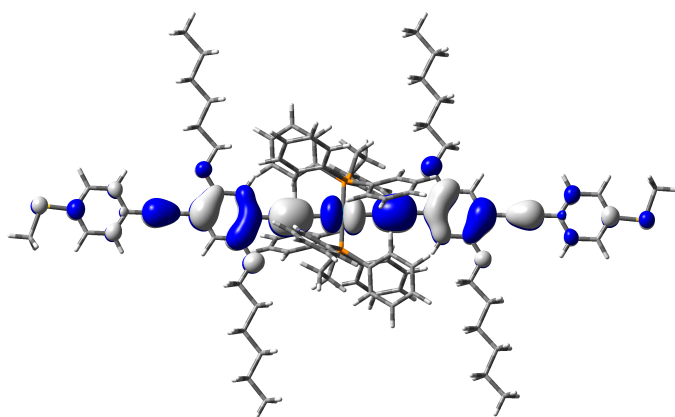
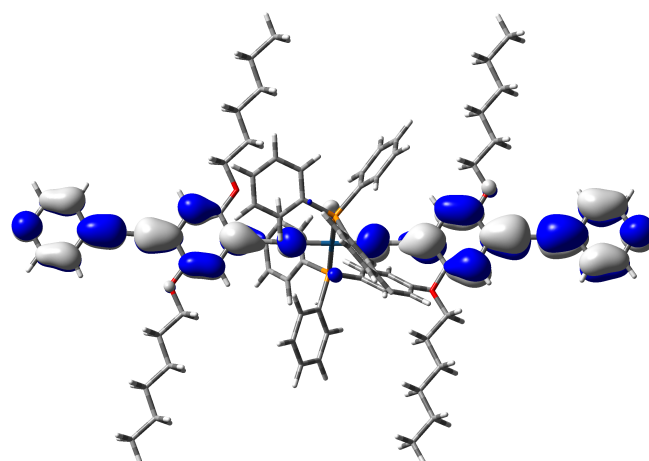
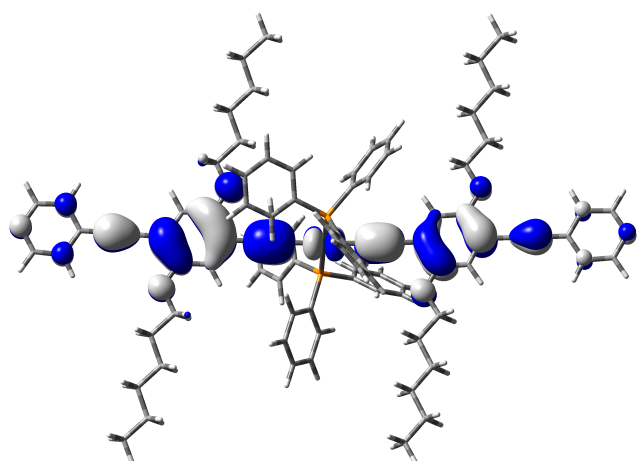
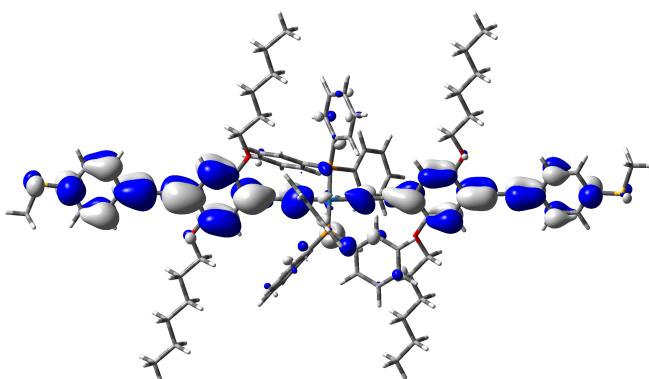
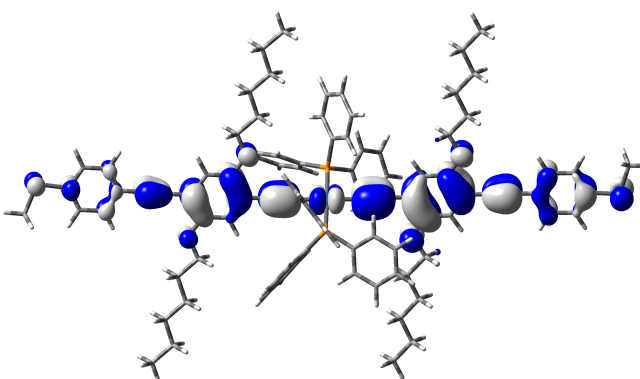






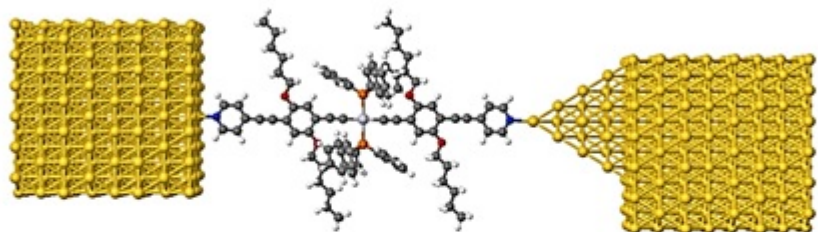
HOMO

LUMO

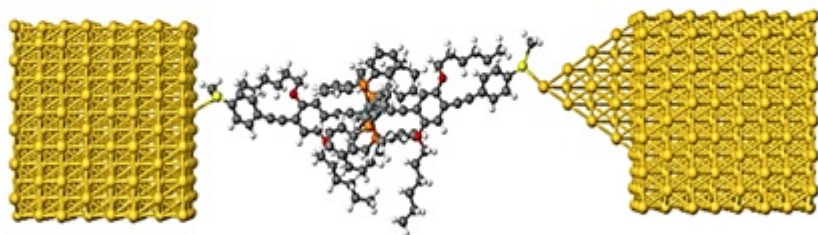
**1-Ru****2-Ru****1-Pt**



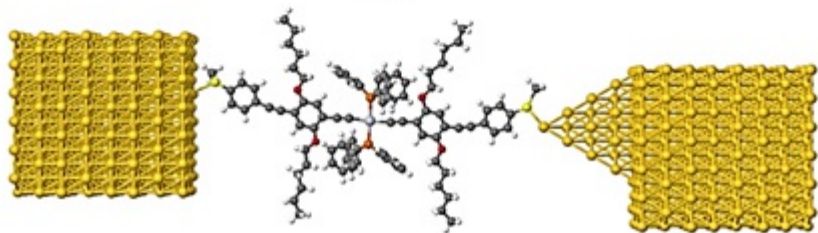
1-Ru



1-Pt



2-Ru



2-Pt

